1521-009X/49/9/844–855$35.00
DRUG METABOLISM AND DISPOSITION

https://doi.org/10.1124/dmd.120.000318
Drug Metab Dispos 49:844–855, September 2021

Leveraging Physiologically Based Pharmacokinetic Modeling and Experimental Data to Guide Dosing Modification of CYP3A-Mediated Drug-Drug Interactions in the Pediatric Population[S]

Sara N. Salerno, Fernando O. Carreño, Andrea N. Edginton, Michael Cohen-Wolkowiez, and Daniel Gonzalez

Division of Pharmacotherapy and Experimental Therapeutics, UNC Eshelman School of Pharmacy, The University of North Carolina at Chapel Hill, Chapel Hill, North Carolina (S.N.S., F.O.C., D.G.); School of Pharmacy, University of Waterloo, Kitchener, ON, Canada (A.N.E.); Duke Clinical Research Institute, Durham, NC, USA (M.C.-W.); Department of Pediatrics, Duke University School of Medicine, Durham, North Carolina (M.C.-W.)

Received November 19, 2020; accepted June 2, 2021

ABSTRACT

Solithromycin is a novel fluoroketolide antibiotic that is both a substrate and time-dependent inhibitor of CYP3A. Solithromycin has demonstrated efficacy in adults with community-acquired bacterial pneumonia and has also been investigated in pediatric patients. The objective of this study was to develop a framework for leveraging physiologically based pharmacokinetic (PBPK) modeling to predict CYP3A-mediated drug-drug interaction (DDI) potential in the pediatric population using solithromycin as a case study. To account for age, we performed in vitro metabolism and time-dependent inhibition studies for solithromycin for CYP3A4, CYP3A5, and CYP3A7. The PBPK model included CYP3A4 and CYP3A5 metabolism and time-dependent inhibition, glomerular filtration, P-glycoprotein transport, and enterohepatic recirculation. The average fold error of simulated and observed plasma concentrations of solithromycin in both adults (1966 plasma samples) and pediatric patients from 4 days to 17.9 years (684 plasma samples) were within 0.5- to 2.0-fold. The geometric mean ratios for the simulated area under the concentration versus time curve (AUC) extrapolated to infinity were within 0.75- to 1.25-fold of observed values in healthy adults receiving solithromycin with midazolam or ketoconazole. DDI potential was simulated in pediatric patients (1 month to 17 years of age) and adults. Solithromycin increased the simulated midazolam AUC 4- to 6-fold, and ketoconazole increased the simulated solithromycin AUC 1- to 2-fold in virtual subjects ranging from 1 month to 65 years of age. This study presents a systematic approach for incorporating CYP3A in vitro data into adult and pediatric PBPK models to predict pediatric CYP3A-mediated DDI potential.

SIGNIFICANCE STATEMENT

Using solithromycin, this study presents a framework for investigating and incorporating CYP3A4, CYP3A5, and CYP3A7 in vitro data into adult and pediatric physiologically based pharmacokinetic models to predict CYP3A-mediated DDI potential in adult and pediatric subjects during drug development. In this study, minor age-related differences in inhibitor concentration resulted in differences in the magnitude of the DDI. Therefore, age-related differences in DDI potential for substrates metabolized primarily by CYP3A4 can be minimized by closely matching adult and pediatric inhibitor concentrations.

Introduction

Per the US Food and Drug Administration (FDA) guidance, drug developers must perform in vitro studies to evaluate drug-drug interaction (DDI) potential for an investigational drug product (https://www.fda.gov/regulatory-information/search-fda-guidance-documents/clinical-drug-interaction-studies-cytochrome-p450-enzyme-and-transporter-mediated-drug-interactions). The FDA recommends routinely evaluating CYP1A2, CYP2B6, CYP2C8, CYP2C9, CYP2C19, CYP2D6, and CYP3A4/5 toward metabolism of the investigational drug, as well as the potential for inhibition of these drug-metabolizing enzymes in both a reversible and time-dependent manner. Relevant in vitro results can be incorporated within static and dynamic models, such as physiologically based pharmacokinetic (PBPK) models, to inform the need for and to guide the design of clinical DDI studies (https://www.fda.gov/regulatory-information/search-fda-guidance-documents/vitro-drug-interaction-studiescytochrome-p450-enzyme-and-transporter-mediated-drug-interactions; https://www.fda.gov/regulatoryinformation/search-fda-guidance-documents/clinical-drug-interaction-studies-cytochrome-p450-enzyme-andtransporter-mediated-drug-interactions) (US Food and Drug Administration, 2020). Clinical DDI studies are typically performed in healthy adults, and

Research reported in this publication was supported by the Eunice Kennedy Shriver National Institute of Child Health and Human Development (NICHD) [Grant 5K23HD083465]. S.N.S. received financial support from the National Institute of General Medical Sciences and the NICHD [Grant T32GM086330]. F.O.C. was funded through a University of North Carolina at Chapel Hill/GlaxoSmithKline Pharmacokinetics/Pharmacodynamics Postdoctoral Fellowship. M.C.-W. received support for research from the National Institutes of Health (NIH) ([Grant 1R01-HD076676-01A1], [Grant 1K24-AI143971]), National Institute of Allergy and Infectious Diseases ([Grant HHSN272201500006I], [Grant HHSN272201300017I]), NICHD [HHSN275201000003I], US Food and Drug Administration [5U18-FD006298], and industry for drug development in adults and children. D.G. received research support from the NICHD ([Grant 5K23HD083465], [Grant 5R01HD096435-03], and [Grant 1R01HD102949-01A1]).

M.C.-W. and D.G. have previously received research support for solithromycin drug development research sponsored by the US Biomedical Advanced Research and Development Authority [HHSO100201300009C], which had a contract with the sponsor to perform the pediatric trials.

https://doi.org/10.1124/dmd.120.000318.

[S] This article has supplemental material available at dmd.aspetjournals.org.

such studies are not routinely performed in pediatric patients for ethical and practical reasons. It is often assumed that DDI potential is the same in pediatric patients as in healthy adults. However, DDI potential may differ in young children relative to adults due to developmental changes in drug-metabolizing enzymes and transporters. In a systematic literature review, fold interactions were compared between 31 pediatric studies and 33 adult studies for 24 drug pairs using clearance, steady-state plasma concentrations, or area under the curve (AUC). Fold interactions were higher (>1.25-fold) or lower (<0.8-fold) in pediatric patients compared to adults for 10 and 8, respectively, out of these 33 cases (Salem et al., 2013). By example, digoxin plus amiodarone and lamotrigine plus valproate resulted in a 2.18-fold higher and 0.58-fold lower exposure, respectively, in pediatric patients compared with adults (Salem et al., 2013). PBPK modeling can account for these developmental changes and can predict DDI potential when pediatric DDI data are unavailable (Grimstein et al., 2019; Lang et al., 2020; Zhang et al., 2020). The objective of this study is to develop a framework for leveraging PBPK modeling to predict metabolic DDI potential in pediatric patients and guide dose adjustments during drug development using solithromycin as a case study.

Solithromycin is a novel fluoroketolide antibiotic that is both a substrate and time-dependent inhibitor of CYP3A4 and thus inhibits its own metabolism. Metabolism experiments using pooled human liver microsomes, CYP450 selective inhibitors, and single cDNA-expressed CYP450s demonstrated that CYP3A4 is the major CYP450 enzyme responsible for the metabolism of solithromycin. However, the contribution of CYP3A5 was not explored. Using pooled human liver microsomes with midazolam as the CYP3A substrate, solithromycin was reported to be a potent CYP3A time-dependent inhibitor with an inactivation rate constant (k_{inact}) and a concentration of half-maximal inactivation (K_I) of 0.022 $minute^{-1}$ and 0.038 μg/ml, respectively (Salerno et al., 2017). However, recombinant studies with CYP3A4, CYP3A5, and CYP3A7 were not performed. Solithromycin is also a P-glycoprotein substrate with an efflux ratio above 10 in Caco-2 cells, which reduced to unity in the presence of inhibitors (10 μM valspodar and 60 μM verapamil) (https://www.fda.gov/advisory-committees/antimicrobial-drugs-advisory-committee-formerly-known-anti-infective-drugs-advisory-committee/briefing-information-november-4-2016-meeting-antimicrobial-drugs-advisory-committee-amdac). Solithromycin undergoes biliary and urinary excretion with 76.5% and 14.1% of the dose recovered in feces and urine, respectively (MacLauchlin et al., 2018). We previously developed a PBPK model for solithromycin in adults, but it did not include CYP3A7, which may be important for predicting DDI potential in infants. Therefore, we determined and incorporated metabolism and time-dependent inhibition parameters for CYP3A4, CYP3A5, and CYP3A7 into an adult and pediatric PBPK model for solithromycin to characterize DDI potential across the pediatric age continuum.

Solithromycin (oral regimen: 800 mg on day 1 followed by 400 mg on days 2–5 and switching from 400 mg intravenous daily to the oral regimen) was noninferior to moxifloxacin for patients with moderately severe community-acquired bacterial pneumonia (CABP) (Barrera et al., 2016; File et al., 2016). However, solithromycin was not approved by the FDA due to concerns of hepatotoxicity, since more patients receiving intravenous-to-oral solithromycin experienced transient asymptomatic transaminitis (Buege et al., 2017). Phase 2 studies in healthy adult volunteers have been performed to assess the DDI potential of solithromycin as a CYP3A inhibitor with midazolam, as well as to assess the impact of the strong CYP3A inhibitor ketoconazole on the pharmacokinetics (PK) of solithromycin. In addition, a phase 1 study was conducted in adolescents with suspected or confirmed bacterial infection receiving oral capsules of solithromycin [12 mg/kg of body weight (800 mg maximum) on day 1 and 6 mg/kg (400 mg maximum) on days 2–5] (Gonzalez et al., 2016). A follow-up phase 1, open-label, multicenter PK and safety study was conducted in children (0–17 years) with suspected or confirmed bacterial infection receiving intravenous and oral (capsules and suspension) solithromycin as add-on therapy (Gonzalez et al., 2018). Using solithromycin as a case study, we will present a guideline for conducting and integrating relevant experimental studies into adult and pediatric PBPK models to predict pediatric CYP3A mediated DDI potential during drug development.

Materials and Methods

High-Performance Liquid Chromatography-Tandem Mass Spectrometry Analysis. High-performance liquid chromatography with tandem mass spectrometry (HPLC/MS/MS) assay was developed for 6β-hydroxytestosterone and the internal standard, 4-androsten-19-1al 3,17-dione (Sigma-Aldrich, St. Louis, MO). The lower limit of quantification for the 6β-hydroxytestosterone assay was 1 μM. The coefficient of variation for the intraday and interday precision was 11% and 7%, respectively (Salerno et al., 2021). Solithromycin was provided at no cost by Melinta Therapeutics, Inc. A Thermo triple stage quadrapolet Quantum Ultra triple-quadrupole mass spectrometer and Waters (Milford, MA) Acquity Ultra Performance Liquid Chromatography charged surface hybrid C18 (1.7 μm, 3 mm × 100 mm) column was used for the solithromycin assay with roxithromycin (Sigma-Aldrich, St. Louis, MO) as the internal standard. An isocratic mobile phase consisted of 2% of 10 mM ammonium bicarbonate and 98% methanol delivered at 350 μl/min for 5 minutes. Calibration standard concentrations (1, 3.3, 10, 33, 100, 333, 1000, and 3333 nM solithromycin plus 0.5 μM roxithromycin) prepared in the same buffer as the experimental samples were used for method validation. A positive mode electrospray ionization was used. Solithromycin and roxithromycin eluted at 2.1 and 3.6 minutes, respectively. The precursor to product ions monitored with corresponding collision energies were 845.3 to 115.8 (36 V), 158.0 (35 V), 656.3 (34 V), 670.3 (29 V), and 688.3 (25 V) for solithromycin and 837.5 to 116.1 (35 V), 158.1 (32 V), and 679.6 (19 V) for roxithromycin. The lower limit of quantification for the solithromycin assay was 1 nM. The mean (range) accuracy was −5% (−15% to 11%). The mean (range) intraday and interday CV was 7% (1%–14%) and 12% (6%–18%), respectively.

Time-Dependent Inhibition of CYP3A Using Recombinant Enzymes. Testosterone was purchased from Sigma-Aldrich (St. Louis, MO). Human CYP3A4, CYP3A5, and CYP3A7 + reductase + cytochrome b5 reductase, 0.5 M phosphate buffer, pH 7.4, and NADPH Regenerating System Solutions A and B were all purchased from Corning Life Sciences (Corning, NY). Experiments were first performed to determine linear 6β-hydroxytestosterone formation (Salerno et al., 2021). Time-dependent inhibition experiments for determination of K_I and k_{inact} were performed in triplicate on two different days. CYP3A4 and CYP3A5 (200 pmol/ml) were preincubated with solithromycin (0, 0.355, 3.55, 10.7, 17.8, 35.5, and 355 μM) at 37°C for 5 minutes in 100 mM potassium phosphate pH 7.4 (200 μl reaction volume). For CYP3A7, 400 pmol/ml of CYP3A7 was preincubated with solithromycin (0, 35.5, 107, 178, 355, and 1065 μM). The reactions were initiated by the addition of NADPH Regenerating System

ABBREVIATIONS: AFE, average fold error; AUC, area under the concentration versus time curve; $AUC_{0-\infty}$, area under the concentration versus time curve extrapolated to infinity; $AUC_{0-\tau}$, area under the concentration versus time curve within a dosing interval; $AUC_{0-24,ss}$, area under the concentration versus time curve from 0 to 24 hours at steady state; CABP, community-acquired bacterial pneumonia; CL, clearance; DDI, drug-drug interaction; FDA, US Food and Drug Administration; HPLC/MS/MS, high-performance liquid chromatography with tandem mass spectrometry; K_I, concentration of half-maximal inactivation; k_{inact}, inactivation rate constant; K_M, concentration at half-maximal velocity; K_{obs}, pseudo first-order rate constant of inactivation; P450, cytochrome P450; PBPK, physiologically based pharmacokinetic; Pi, input parameter; ΔPKj, change in the pharmacokinetic parameter estimate; PK, pharmacokinetics; PMA, postmenstrual age; PopPK, population PK; UGT1A1, uridine diphosphate glucuronosyltransferase 1A1.

Solutions A and B at a dilution of 1:20 and 1:100, respectively. The protein content in the reactions was 1.6 mg/ml. After 0, 2.5, 5, 10, 15, and 30 minutes for CYP3A4 and CYP3A5 and 0, 5, 15, 30, 45, and 60 minutes for CYP3A7, 10-μl aliquots were diluted 10-fold into 90 μl of fresh buffer containing 100 mM potassium phosphate pH 7.4 and NADPH regenerating system plus 250 μM testosterone. The secondary reactions were incubated at 37°C for 5 minutes for CYP3A4 and CYP3A5 and 30 minutes for CYP3A7, and then reactions were stopped by a 1:4 dilution into ice-cold acetonitrile containing 0.5 μM 4-androsten-19-1al 3,17-dione. The samples were centrifuged at 3500 rotations per minute for 10 minutes at 4°C, and the supernatant was removed, and 6β-hydroxy-testosterone was measured to estimate remaining enzymatic activity.

To determine the K_I and k_{inact}, first, the percent activity remaining was calculated according to eq. 1, where $A_{inactivator}$ is the enzymatic activity of the inactivator, $A_{vehicle}$ is the enzymatic activity of the vehicle control, $T_{0,\ NADPH}$ is the 0-minute preincubation time, and $T_{min,\ NADPH}$ is the preincubation measured at different time intervals (Grimm et al., 2009).

$$\%\ \text{activity} = 100 \times \left[\left(\frac{A_{inactivator}}{A_{vehicle}}\right) at\ T_{0,\ NADPH} - \left(\frac{A_{inactivator}}{A_{vehicle}}\right) at\ T_{min,\ NADPH}\right] \quad (1)$$

The natural log of the percent activity remaining was plotted against preincubation time, and the negative slope, which is the pseudo first-order rate constant of inactivation (K_{obs}), was determined using linear regression within GraphPad Prism version 8 (GraphPad Software, San Diego, CA). Finally, the K_{obs} was determined for solithromycin by performing nonlinear regression in GraphPad Prism version 8 according to eq. 2, where I is the inactivator (solithromycin) concentration.

$$K_{obs} = \frac{K_{inact} \times [I]}{K_I + [I]} \quad (2)$$

Solithromycin CYP3A In Vitro Metabolism Using Recombinant Enzymes. Pilot experiments were first performed to determine the linear range of disappearance of solithromycin. CYP3A4 and CYP3A5 (60 pmol/ml) were incubated with 1 μM solithromycin in 100 mM potassium phosphate pH 7.4 plus NADPH Regenerating System Solutions A and B at a dilution of 1:20 and 1:100, respectively, for 0, 2, 5, 10, 15, 30, and 60 minutes. CYP3A7 (100 pmol/ml) was incubated with 1 μM and 10 μM of solithromycin for 0, 5, 10, 15, 20, 30, and 60 minutes. CYP3A7 (100 pmol/ml) was also incubated with 250 μM testosterone for 0, 15, 30, and 60 minutes as a positive control. The reactions were stopped by a 1:5 dilution into ice-cold methanol containing 0.5 μM roxithromycin (or acetonitrile containing 0.5 μM 4-androsten-19-1al 3,17-dione), centrifuged at 3500 rpm for 10 minutes at 4°C, and solithromycin and 6β-OH-testosterone were measured in the supernatant by HPLC/MS/MS.

Metabolism experiments for determination of the maximal velocity (V_{max}) and the concentration at half the maximal velocity (K_M) were performed in triplicate on three different days. CYP3A4 and CYP3A5 (60 pmol/ml) were preincubated with solithromycin (0.005, 0.01, 0.05, 0.1, 0.25, 0.5, 1, 2, 3, 4, 5 μM for CYP3A4 and 0.01, 0.05, 0.1, 0.25, 0.5, 1, 2, 3, 4, 5, 10, 30 μM for CYP3A5) at 37°C for 5 minutes in 100 mM potassium phosphate pH 7.4 plus NADPH Regenerating System Solutions A and B at a dilution of 1:20 and 1:100, respectively (200 μl reaction volume). The third experiment for CYP3A5 was conducted at higher concentrations (30, 50, 100, 500 1000, 3700 μM) to further characterize the V_{max}. The reactions were initiated by the addition of 12 μl (12 pmol) Corning Supersomes. Samples were collected at 0 minutes and 2 minutes for CYP3A4 and 15 minutes for CYP3A5. Reactions were stopped by a 1:2 to 1:1000 dilution into ice-cold methanol to ensure concentrations were within the assay range from 0.001 to 3.333 μM). The samples were centrifuged at 3500 rpm for 10 minutes at 4°C, and the supernatant was removed, and then evaporated to remove the methanol. Samples were resuspended in 98% methanol plus 2% of 10 mM ammonium bicarbonate containing 0.5 μM roxithromycin and then analyzed by HPLC/MS/MS. Solithromycin metabolite formation was calculated by subtraction of concentrations at the final time from the initial time. Finally, the K_M and V_{max} were determined by nonlinear regression in GraphPad Prism 8 using the Michaelis-Menten least-squares fit using eq. 3 where [S] is solithromycin concentration (http://www.graphpad.com/guides/prism/7/statistics/index.htm).

$$Velocity = \frac{V_{max} * [S]}{K_M + [S]} \quad (3)$$

Adult Solithromycin PBPK Model Development and Evaluation. The generic model structure implemented within PK-Sim includes 15 organs/tissues and blood pool compartments (Supplemental Material). A whole-body adult PBPK model was developed and evaluated in PK-Sim (version 9.0; Open Systems Pharmacology Suite) using plasma concentration data from 100 healthy subjects and 22 patients with CABP (1966 plasma samples) (Supplemental Table 1) (Salerno et al., 2017). A mean virtual individual was used for model development based on demographics of the clinical study in healthy adults: a 44.7-year-old Black American man with a weight of 85.6 kg and a height of 180.9 cm. The model included glomerular filtration, CYP3A4 and CYP3A5 metabolism, time-dependent inhibition, P-glycoprotein transport, and enterohepatic recycling. The relative organ concentrations of P-glycoprotein and CYP3A were taken from the built-in database query, thereby allowing one set of kinetic parameters to be used in all organs (Meyer et al., 2012). In brief, PK-Sim uses a gene expression database to determine protein abundances in the organ/tissue compartments, and catalytic activity is calculated in each organ/tissue using a global kinetic value. Therefore, catalytic activity for P-glycoprotein and CYP3A will be accounted for in any organ/tissue that expresses these proteins. Solithromycin was 78% to 84% bound to adult human plasma, primarily to serum albumin, and the extent of protein binding was not concentration dependent. Therefore, protein binding was mediated through albumin with a fraction unbound of 0.22. The partition coefficients for tissues and organs are deduced in PK-Sim from physicochemical properties including protein binding and lipophilicity. Tissue-to-plasma partition coefficients predicted using the Berezhkovsky algorithm best characterized the data and cellular permeability was calculated using the PK-Sim standard algorithm (Berezhkovskiy, 2004; https://docs.open-systems-pharmacology.org/working-with-pk-sim/pk-sim-documentation). The solithromycin CYP3A4/CYP3A5 K_M and K_I were corrected for protein binding based on the equation: fraction of drug concentration unbound is equal to 1/(1 + C*10^(0.072*log P^2 + 0.067*log P − 1.126), where C was the protein concentration (Hallifax and Houston, 2006). Lipophilicity and P-glycoprotein V_{max} were manually optimized using the intravenous data. Transcellular intestinal permeability and the Weibull oral distribution properties (dissolution time of 90 minutes and dissolution shape of 1.50) were manually optimized using the oral data. All other parameters were obtained from the literature or were experimentally generated (Table 1).

Population simulations were performed with 100 virtual Black American subjects with demographics from study CE01-102 in healthy adults: 27% female with a mean (range) age of 32.9 (20–55) years and a weight of 74.5 (61.4–90.3) kg. Population variability for P-glycoprotein was introduced using a normal distribution with a 65% coefficient of variation (Harwood et al., 2013). The PBPK model was evaluated by comparing the C_{max}, area under the concentration versus time curve extrapolated to infinity ($AUC_{0-\infty}$) or during a dosing interval ($AUC_{0-\tau}$), and clearance (CL) between the observed data and the PBPK model simulations on day 1 and at steady state following multiple daily dosing. The relative accuracy was calculated as a ratio of mean predicted values over mean observed values with a ratio assessed for the standard deviation (S.D.) (Jiang et al., 2013; Johnson et al., 2014; Zhou et al., 2016).

$$Ratio\ for\ SD = \sqrt{\left(\frac{sd\ (observed)}{mean\ (observed)}\right)^2 + \left(sd\ \left(\frac{predicted}{mean\ (predicted)}\right)\right)^2} \times \frac{mean\ (predicted)}{mean\ (observed)} \quad (4)$$

The average fold error (AFE) was also calculated for each dosing regimen using the simulated geometric mean according to eq. 5, where n is the sample size:

$$AFE = 10^{\left(\frac{1}{n}\right) * \sum log\left(\frac{predicted}{observed}\right)}. \quad (5)$$

Model performance was assessed with a visual predictive check and by calculating the percentage of model-predicted concentrations and PK parameters falling within 2-fold, 1.5-fold, and 1.33-fold predictive error.

Sensitivity Analysis. Sensitivity analysis was performed for a 45-year-old male receiving 800 mg, oral administration, day 1 followed by 400 mg, oral administration, days 2–5. In PK-Sim, the input parameter (Pi) is varied around the value in the simulation by a small change, and a new simulation is performed, keeping all other input values constant. The change in the PK parameter estimate (ΔPKj) is calculated as the difference between the values in the new simulation and the original simulation. The sensitivity for the PK parameter to the input parameter is calculated as the ratio of the relative change of that PK parameter (ΔPKj/PKj) and the relative variation of the input parameter (ΔPi/Pi): (ΔPKj/ΔPi)*(Pi/PKj) (https://docs.open-systems-pharmacology.org/working-with-pk-sim/pk-sim-documentation). Parameters with sensitivity values <-0.5 or >0.5 were

TABLE 1

Final PBPK model parameters for solithromycin, ketoconazole, and midazolam

Parameter	Solithromycin	Source	Ketoconazole	Source	Midazolam	Source
Molecular weight (g/mol)	845.01	*a*	531.44	(DrugBank.DrugBank 5.0, 2018)	325.77	(DrugBank.DrugBank 5.0, 2018)
Log P	4.04	*a*	2.44	*b*	2.76	b
Compound type	Base	*a*	Base	(DrugBank.DrugBank 5.0, 2018)	Base	(DrugBank.DrugBank 5.0, 2018)
pKa	9.44	*a*	2.90, 6.50	(DrugBank.DrugBank 5.0, 2018)	6.57	(DrugBank.DrugBank 5.0, 2018)
Solubility (mg/ml)	0.40	*a*	$9.31 * 10^{-3}$	(DrugBank.DrugBank 5.0, 2018)	0.01	(DrugBank.DrugBank 5.0, 2018)
Fraction unbound[d]	22%	*a*	2% (100 mg) 1% (200, 400 mg) 0.75% (800 mg)	*b* (DrugBank.DrugBank 5.0, 2018) *b*	3%	(DrugBank.DrugBank 5.0, 2018)
UGT1A1 K_M (μM)	N/A	N/A	22.3	(Bourcier et al., 2010)	N/A	N/A
UGT1A1 V_{max} (mg/protein/min)	N/A	N/A	9366	*b*	N/A	N/A
CYP3A4 K_M (μM)	0.14 (e)	*c*	235	(Hyland et al., 2003)	1.88	(Xiao et al., 2019)
CYP3A4 V_{max} (pmol/min/pmol)	3.44	*c*	0.90	*b*	6.12	(Xiao et al., 2019)
CYP3A5 K_M (μM)	13.3 (e)	*c*	N/A	N/A	N/A	N/A
CYP3A5 V_{max} (pmol/min/pmol)	23.4	*c*	N/A	N/A	N/A	N/A
CYP3A4 k_{inact} (1/min)	0.08	*c*	N/A	N/A	N/A	N/A
CYP3A4 K_I (μM)	0.41 (e) (TDI)	*c*	0.0038 (Competitive)	(Von Moltke et al., 1996)	N/A	N/A
CYP3A5 k_{inact} (1/min)	0.03	*c*	N/A	N/A	N/A	N/A
CYP3A5 K_I (μM)	0.71 (e) (TDI)	*c*	0.109 (Noncompetitive)	(Gibbs et al., 1999)	N/A	N/A
P-glycoprotein K_M (μM)	45	(Pachot et al., 2003)	N/A	N/A	N/A	N/A
P-glycoprotein V_{max} (μmol/L/min)	1.24	*b*	N/A	N/A	N/A	N/A
P-glycoprotein K_I (ng/mL)	N/A	N/A	2.27	(Oishi et al., 2018)	N/A	N/A
Transcellular intestinal permeability (cm/min)	$8 * 10^{-5}$	*b*	$3.14 * 10^{-3}$ (adult) $2 * 10^{-4}$ (pediatric)	*b* *b*	$1.25 * 10^{-5}$	*b*

[a]Sponsor data on file.
[b]Optimized value.
[c]Experimentally derived.
[d]Based on adult data.
[e]Corrected for protein binding based on the equation: fraction of drug concentration unbound is equal to 1/(1+C*10∘(0.072*log P^2+0.067*log P-1.126), where C was the protein concentration (Hallifax and Houston, 2006).
K_M, Michaelis-Menten constant; N/A, not applicable; P-gp, P-glycoprotein; TDI, time-dependent inhibition; K_I: inhibition constant; k_{inact}: maximal inactivation rate constant; V_{max}: maximal rate of metabolism.

reported for the steady-state half-life. A sensitivity value −0.5 or 0.5 indicates that a 5% increase of the parameter leads to a 10% decrease or increase of the PK parameter value, respectively.

Solithromycin DDI Predictions in Healthy Adult Volunteers. The solithromycin and midazolam PBPK models were comodeled based on the previously described drug properties, which included CYP3A4 and CYP3A5 time-dependent inhibition (Supplemental Material; Table 1). Healthy adults (21–54 years of age) received oral solithromycin (400 mg on days 3–7 in one period and 800 mg day 3 followed by 400 mg on days 4–7 in another period) in combination with oral midazolam 0.075 mg/kg given on days 1, 3, and 7 of each period (sponsor data on file). Simulations were also performed and compared with observed data in healthy adults receiving solithromycin in combination with ketoconazole incorporating CYP3A4 and CYP3A5 time-dependent inhibition by solithromycin, in addition to CYP3A4 and P-glycoprotein reversible inhibition by ketoconazole (Supplemental Material; Table 1). Healthy adults (23–54 years of age) received a single oral dose of solithromycin (400 mg on day 1), a 5-day washout period, 4 days of oral ketoconazole (400 mg alone on days 7–10), and then 400 mg oral solithromycin plus ketoconazole on day 11. We calculated the geometric mean ratio for C_{max} and $AUC_{0-\infty}$ along with the associated 90% confidence interval for the drug combinations (solithromycin plus ketoconazole or solithromycin plus midazolam) relative to solithromycin or midazolam alone.

Pediatric PBPK Model Development and Evaluation. A virtual 32-year-old White male was scaled to a virtual 7.56-year-old child based on the mean pediatric solithromycin data using anthropomorphic and ontogeny functions. Clearance was scaled using the PK-Sim default sigmoidal maturation equations, where A is the relative activity at a postmenstrual age (PMA) in weeks, $A_{0.5}$ is the PMA in weeks at 50% activity compared with an adult, and n is the Hill coefficient (eq. 6) (PK-Sim, 2017). Variability in the ontogeny was also introduced by simulating a virtual population with 10000 individuals and then fitting the geometric mean and geometric S.D. around all of the fitted parameters (PK-Sim, 2017). CYP3A5 has an ontogeny factor of 1 for all ages (Stevens et al., 2003).

The ontogeny function for CYP3A4 in the liver (eq. 7) was derived using the following literature data: mRNA expression data and testosterone and dehydoepiandrosterone hydroxylation activity obtained from human livers in fetuses 14–40 weeks, children 1 day to 9 years, and adult donors for transplantation (Lacroix et al., 1997); formation of amprenavir metabolites in human liver microsomes obtained from a fetus, neonate at 1 day, neonate at 2 days, infant at 1 month, infant at 3 months, and an adult (Tréluyer et al., 2003); and CYP3A4 expression levels in 77 fetal and pediatric liver microsome samples from 217 to 287 estimated gestational age and 3 to 6 months postnatal age (Stevens et al., 2003). The ontogeny function for CYP3A4 in the intestine (eq. 8) was based upon duodenal biopsies and surgical sections collected in 104 pediatric patients ranging from 2 weeks to 17 years as well as 11 fetuses. CYP3A4 expression was assessed by Western blotting and by immunohistochemistry as well as the rate of formation of 6β-hydroxytestosterone from testosterone (Johnson et al., 2001).

The ontogeny function for CYP3A4 within PK-Sim had 50% activity compared with adults at 73.019 weeks PMA (0.63 years postnatal age). This value is comparable, albeit slightly lower than the value of 108 weeks postmenstrual age (1.3 years postnatal age) in the ontogeny function derived by Salem, et al. (2014). In brief, Salem, et al. (2014) developed an ontogeny function for CYP3A based on in vivo pharmacokinetic data for midazolam reported in the literature adjusting for critically ill pediatric subjects receiving mechanical ventilation.

TABLE 2

Time-dependent inhibition and Michaelis-Menten kinetic parameters.

Data are presented as the mean (95% confidence interval) fitted using GraphPad Prism version 8.0 based on triplicates from two different dates for time-dependent inhibition parameters and from three different dates for Michaelis-Mentin parameters.

Enzyme	k_{inact}	K_I	K_M	V_{max}
	1/min	*μg/ml*	*μM*	*pmol/min/pmol CYP3A*
CYP3A4	0.084 (0.078, 0.092)	1.49 (0.96, 2.26)	0.60 (462, 781)	3.44 (3.21, 3.71)
CYP3A5	0.029 (0.026, 0.032)	2.61 (1.52, 4.15)	57.8 (41.8, 87.8)	23.4 (18.7, 32.0)

Another CYP3A ontogeny function was developed by Upreti, et al. (2016) based on human clinical data reported in the literature for sufentanil with 50% activity compared with adults at 0.10 years.

The default ontogeny function for CYP3A7 (eq. 9) in PK-Sim was derived using the following literature data: mRNA expression data and testosterone and dehydroepiandrosterone hydroxylation activity obtained from human livers in fetuses 14–40 weeks, children 1 day to 9 years, and adult donors for transplantation (Lacroix et al., 1997); and CYP3A7 expression levels in 77 fetal and pediatric liver microsome samples from 217 to 287 estimated gestational age and 3 to 6 months postnatal age (Stevens et al., 2003). The ontogeny function for CYP3A7 is shown in eq. 3, although not needed in this study because solithromycin was not a significant substrate for CYP3A7.

The ontogeny function for uridine diphosphate glucuronosyltransferase 1A1 (UGT1A1) (eq. 10) was derived using liver bilirubin glucuronidation data toward eight substrates in fetal term and adult postmortem (less than 5 hours after death) liver samples (Burchell et al., 1989). In another study, bilirubin UDP-glycuronyltransferase activities were assessed in 70 liver samples obtained from 30 newborns, 20 of which were premature, as well as 21 infants, 5 children, and 14 adults (Onishi et al., 1979).

P-glycoprotein expression was calculated as a function of postnatal age and then normalized to mean adult expression based upon data quantified using 69 human pediatric and 41 adult livers (eq. 10) (Prasad et al., 2016). This ontogeny function for P-glycoprotein expression was applied to both the liver and intestine. Protein binding to albumin was scaled according to the default ontogeny factor within PK-Sim (eq. 12).

$$A = \frac{\mathrm{PMA}^{n}}{A_{0.5}{}^{n} + \mathrm{PMA}^{n}} \tag{6}$$

$$CYP3A4\ ontogeny\ factor\ in\ liver = \frac{PMA^{3.331}}{73.019^{3.331} + PMA^{3.331}} \tag{7}$$

$$CYP3A4\ ontogeny\ factor\ in\ intestine = \frac{PMA^{1.237}}{74.055^{1.237} + PMA^{1.237}} \tag{8}$$

$$CYP3A7\ ontogeny\ factor = 1 - \frac{PMA^{27.615}}{48.051^{27.615} + PMA^{27.615}} + 0.0253 \tag{9}$$

$$UGT1A1\ ontogeny\ factor = \frac{PMA^{20.67}}{50.754^{20.67} + PMA^{20.67}} \tag{10}$$

$$P-glycoprotein\ expression(fmol/\mu g\ membrane\ protein)\ at\ age\ (years) = 0.15 + \frac{0.41 * Age^{0.78}}{2.94^{0.78} + Age^{0.78}} \tag{11}$$

$$Albumin\ ontogeny\ factor = \frac{PMA^{3.24}}{21.533^{3.24} + PMA^{3.24}} \tag{12}$$

The intrinsic CL (CL_{int}) for CYP3A4 and CYP3A5 were normalized with respect to the nominal specific content of the corresponding P450 in native human liver microsomes, which was 108 and 1.0 pmol P450/mg microsomal protein for CYP3A4 and CYP3A5, respectively (Rodrigues, 1999). The CL_{int} per organ (μl/min/organ) is the sum of the V_{max}/K_M of each P450 (μl/min/μmol P450) multiplied by the reference concentration (μmol P450/L organ), relative expression, ontogeny factor, and organ volume (L). The reference concentration is the molar concentration of the protein in the organ with the highest enzyme contribution (typically the liver) and expression in other organs is scaled by their

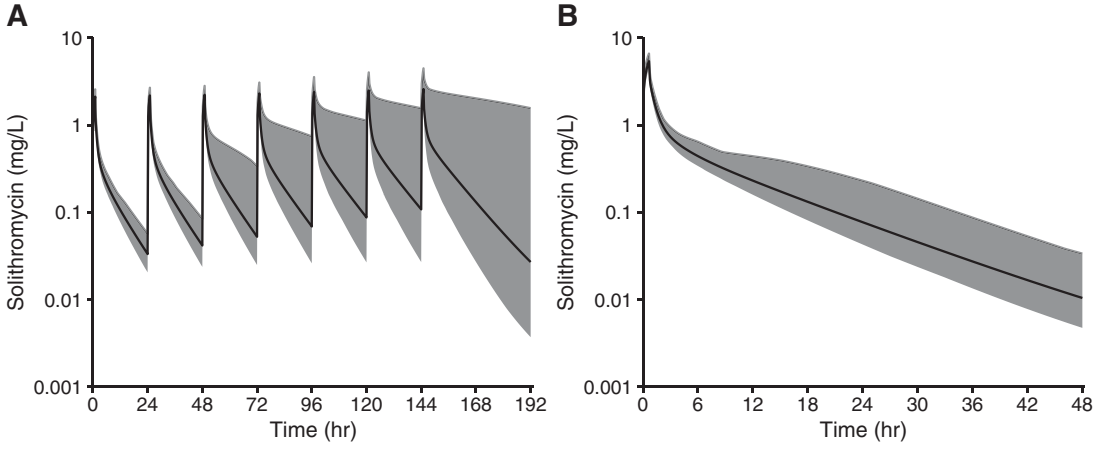

Fig. 1. Population simulations depicting solithromycin concentration (mg/L) versus time in hours (hr) after first dose after solithromycin intravenous administration in healthy adults. Population simulations were performed for 100 virtual subjects using a Black American population with demographics from study CE01-102 for healthy subjects: 27% female with a mean (range) age of 32.9 (20–55) years and a weight of 74.5 (61.4–90.3) kg. (A) 400 mg intravenously daily × 7 days administered over a 60-minute infusion; (B) 800 mg intravenous single dose administered over a 40-minute infusion. The solid gray region is the 90% prediction interval, the solid black line is the simulated geometric mean, and black dots are observed data from subject. The AFE was calculated as $10^{(\frac{1}{n})*\Sigma log(\frac{predicted}{observed})}$, where the predicted values were the simulated geometric mean values and n was the sample size. The AFE was 1.0 and 0.7 for the 400 mg intravenous and 800 mg intravenous plots, respectively.

TABLE 3

Comparison of C_{max} and $AUC_{0\text{-}\tau}$ in adults for solithromycin between observed data and PBPK model simulations.
Data are presented as the mean ± S.D. Overall, 50%, 60%, and 85% of simulated C_{max} or AUC values were within 1.33-, 1.5-, and 2.0-fold of the observed values reported in adults.

Dosing Regimen	Day	C_{max}			$AUC_{0\text{-}\tau}$ or $AUC_{0\text{-}\infty}$		
		Observed (μg/mL)	Simulated (μg/ml)	Ratio	Observed (μg*h/ml)	Simulated (μg*h/ml)	Ratio
400 mg i.v., 60-minute infusion, daily for 7 days	7	2.2 ± 0.44	2.7 ± 0.95	1.2 ± 0.5	13 ± 4.38	15 ± 16	1.2 ± 1.3
800 mg i.v., 40-minute infusion, single dose	1	2.9 ± 0.54	5.4 ± 0.68	1.9 ± 0.4	19 ± 4.79	13 ± 6.63	0.70 ± 0.39
200 mg oral daily for 7 days	1	0.11 ± 0.05	0.23 ± 0.03	2.1 ± 1.0	0.84 ± 0.41	1.4 ± 0.23	1.72 ± 0.88
	7	0.25 ± 0.08	0.27 ± 0.09	1.1 ± 0.5	2.3 ± 0.77	1.9 ± 1.2	0.83 ± 0.59
400 mg oral daily for 7 days	1	0.58 ± 0.37	0.48 ± 0.06	0.8 ± 0.5	4.8 ± 3.1	3.0 ± 0.5	0.63 ± 0.42
	7	1.1 ± 0.52	1.2 ± 0.94	1.1 ± 1.0	13 ± 7.4	13 ± 16	1.0 ± 1.4
600 mg oral daily for 7 days	1	0.86 ± 0.53	0.72 ± 0.09	0.84 ± 0.53	7.7 ± 4.6	4.8 ± 1.3	0.63 ± 0.41
	7	1.5 ± 0.40	3.0 ± 1.5	2.4 ± 1.3	18 ± 5.6	54 ± 34	3.0 ± 2.0
800 mg oral, day 1, 400 mg oral, day 2–5	1	1.5 ± 0.55	1.1 ± 0.17	0.71 ± 0.28	21 ± 9.4[a]	10 ± 9.2[a]	0.53 ± 0.45
	5	1.2 ± 0.36	1.2 ± 0.93	1.0 ± 0.86	17 ± 7.2	13 ± 16	0.80 ± 1.0

[a]Data are reported as the area under the concentration versus time curve from 0 to infinity (AUC_{∞}). The ratio was calculated as the ratio of mean predicted values over mean observed values ± the ratio for the S.D. as described previously (Jiang et al., 2013; Johnson et al., 2014; Zhou et al., 2016).

relative expression. CYP3A4 is mainly expressed in the liver of human adults, some in the gastrointestinal tract, and minor amounts are expressed in almost all other tissues. Hence, the relative expression of CYP3A4 is 100% in the liver (with a reference concentration of 4.32 μmol/L) and 7% in the intestine. For example, the CL_{int} for CYP3A4 in adult liver would be calculated as 61.4 μl/min (5.73 μmol/min/μmol CYP3A4 × 4.32 μmol/L x 2.48 L liver), since the ontogeny factor and relative expression are both 1 for CYP3A4 in adult liver. Similarly, the CL_{int} for CYP3A4 in adult small intestine would be calculated as 1.32 μl/min (5.73 μmol/min/μmol CYP3A4 × 4.32 μmol/L x 0.07 × 0.76 L intestine).

The solithromycin pediatric PBPK model was evaluated using a total of 684 plasma samples available from 96 pediatric patients ranging from 4 days to 17.9 years after excluding 96 samples below the lower limit of quantification. These data were derived from two phase 1 studies, the first of which was conducted in adolescents with suspected or confirmed bacterial infection receiving oral capsules of solithromycin (12 mg/kg of body weight [800 mg maximum] on day 1 and 6 mg/kg [400 mg maximum] on days 2–5) (Gonzalez et al., 2016). A follow-up phase 1, open-label, multicenter PK and safety study was conducted in children (0–17 years) with suspected or confirmed bacterial infection receiving intravenous and oral administration (capsules and suspension) solithromycin as add-on therapy (Gonzalez et al., 2018). A virtual population of 100 pediatric subjects (4 days to 17.9 years of age) was used for model evaluation. Pediatric simulations were performed for these 100 virtual pediatric subjects receiving intravenous, oral suspension, and oral capsules of solithromycin. The solithromycin oral suspension was modeled as a solution (e.g., instantaneous dissolution), whereas the oral capsules were modeled using the Weibull function as fit using the adult data. Solithromycin plasma concentration data were normalized by dose and time relative to the last drug administration since dose, because administration differed slightly for each individual. We also compared weight-normalized CL values from the PBPK simulation to the individual empirical Bayesian post hoc parameter estimates based on a published population PK (PopPK) model developed using plasma data from these same 96 children. The PopPK model was a 2-compartment model with linear elimination and first-order absorption with a oral absorption lag time. Significant covariates included weight and a sigmoidal maturation function for PMA on CL and weight on the volume of distribution (V). Modeling time-dependent inhibition did not improve the model fits in these pediatric patients using a PopPK approach (Gonzalez et al., 2018).

Solithromycin Plus Midazolam Pediatric Simulations. We focused on intravenous solithromycin to rule out the confounding effect of oral formulation (capsules vs. oral suspension) for solithromycin and any age-related differences in absorption. Since the inhibitor concentration influences the magnitude of the DDI, we simulated intravenous doses (60-minute infusion) for solithromycin from ages from 1 month to 17 years of age that achieved similar $AUC_{0\text{-}24,ss}$ as the simulated healthy adult population receiving 400 mg intravenous daily (400 mg maximum). Since there were only two neonates who received solithromycin, we focused on term infants >1 month of age. Dosing simulations were performed for 500 virtual subjects in each age group (1 month to <6 months, 6 months to <2 years, 2 years to <6 years, 6 years to <12 years, 12 to 17 years of age, and 18 to 65 years of age). Midazolam dosing was based upon the recommended intravenous starting dose in the package insert for sedation, anxiolysis, and amnesia prior to procedure in pediatric patients >6 months and healthy adults <60 years of age, as well as the loading dose for sedation/anxiolysis/amnesia in critical care settings for non-neonatal infants between 1 and 6 months (https://online.lexi.com/lco/action/login?reauth; Lexicomp, 2020). We simulated a single dose of midazolam administered alone (day 1) and on the last day of solithromycin daily dosing for 5 days (day 6). The geometric mean ratio and associated 90% confidence interval for midazolam $AUC_{0\text{-}\infty}$ and C_{max} were calculated for midazolam plus solithromycin relative to midazolam alone. Since the P-glycoprotein ontogeny function is based on protein quantification and not functional data, we simulated the DDI with and without the incorporation of the P-glycoprotein ontogeny function in children <6 years of age.

Solithromycin Plus Ketoconazole Pediatric Simulations. Ketoconazole oral dosing in pediatric patients ≥2 years and adults were based upon recommendations in the package insert: 3.3 mg/kg once daily (200-mg maximum) and 200 mg, oral administration, once daily, respectively (Teva, 2014; Lexicomp, 2020).

TABLE 4

Comparison of adult DDI simulations and observed data for solithromycin plus midazolam or ketoconazole.

Treatment Group	Geometric Mean [90% CI] C_{max} Ratio		Geometric Mean [90% CI] $AUC_{0\text{-}\infty}$ Ratio	
	Observed	Simulated	Observed	Simulated
Solithromycin (400 mg daily × 5 days) plus midazolam[a]	2.45 [2.16–2.77]	2.82 [2.72–2.93]	8.96 [7.82–10.3]	9.77 [7.76–12.3]
Solithromycin (800 mg × 1, 400 mg daily × 4 days) plus midazolam[b]	2.45 [2.16–2.77]	3.09 [2.97–3.21]	9.09 [7.92–10.4]	13.8 [10.7–17.7]
Solithromycin (400 mg) plus Ketoconazole (400 mg)[c]	1.56 [1.39–1.76]	1.91 [1.88–1.95]	2.55 [2.24–2.91]	2.30 [2.25–2.36]

[a]Midazolam 0.075 mg/kg, oral, on days 1, 3, and 7 and solithromycin 400 mg once daily (oral) on days 3 to 7. The ratio was calculated for midazolam on day 7 compared with day 1.
[b]Midazolam 0.075 mg/kg (oral) on days 1, 3, and 7 and solithromycin 800 mg (oral) on day 3 followed by 400 mg once daily (oral) on days 4 to 7. The ratio was calculated for midazolam on day 7 compared with day 1.
[c]Solithromycin 400 mg (oral) on day 1 followed by a 5-day washout period, and then 4 days of ketoconazole 400 mg (oral; days 7–10), with solithromycin and ketoconazole oral administration (400 mg each) on day 11. The ratio was calculated for solithromycin on day 11 compared with day 1.

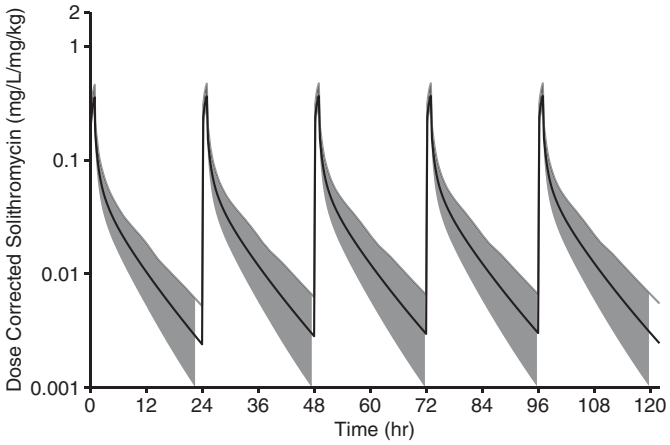

Fig. 2. Population simulations for solithromycin depicting concentration versus time in hours (hr) after the first dose of solithromycin intravenous administration in pediatric patients. Pediatric population simulations for 100 virtual White American subjects from 4 days to 17.9 years of age receiving 1 mg/kg intravenous solithromycin. The solid gray region is the 90% prediction interval, the solid black line is the simulated arithmetic mean line, and the black dots are observed data from pediatric subjects. Solithromycin plasma concentration data were normalized by dose and time relative to the last drug administration since dose and administration differed slightly for each individual.

Given the lack of information in children <2 years of age, we simulated ketoconazole dosing in this population that would result in similar $AUC_{0\text{-}24,ss}$ as the simulated children and adults receiving 3.3 mg/kg or 200 mg, oral daily, respectively. Solithromycin intravenous dosing in pediatric patients (60-minute infusion) were used that achieved similar $AUC_{0\text{-}24,ss}$ as in observed and simulated healthy adults receiving 400-mg intravenously daily (400-mg maximum). We simulated solithromycin administered intravenously alone for 5 days and after 5 days of dosing in combination with oral ketoconazole. The geometric mean ratio and associated 90% confidence interval for solithromycin $AUC_{0\text{-}\infty,ss}$ and C_{max} at steady state ($C_{max,ss}$) were calculated for solithromycin plus ketoconazole administered concurrently for 5 days, relative to solithromycin administered alone for 5 days. Since the P-glycoprotein ontogeny function is based on protein quantification and not functional data, we simulated the DDI with and without the incorporation of the P-glycoprotein ontogeny function in children <6 years of age.

Results

Time-Dependent Inhibition of CYP3A Using Recombinant Enzymes. The time-dependent inhibition parameters (k_{inact} and K_I) for CYP3A4 and CYP3A5 are presented in Table 2, and in Supplemental Figs. 1 and 2. CYP3A7 was not a significant time-dependent inhibitor at concentrations up to 150 μg/ml for preincubation times up to 60 minutes (Supplemental Fig. 3). Reversible inhibition of CYP3A7 was observed at solithromycin concentrations >300 μg/ml, but time-dependent inhibition was not observed (Supplemental Fig. 3). Preincubation times beyond 60 minutes could not be explored because of the loss of recombinant enzyme activity associated with longer incubation times. Additionally, greater dilutions could not be implemented, since the maximum quantity of CYP3A7 was added in the preincubation reaction, and the remaining velocity was approaching the lower limit of detection for 6β-hydroxy-testosterone. Therefore, CYP3A7 time-dependent inhibition parameters could not be generated, and deemed clinically insignificant, for solithromycin.

Solithromycin CYP3A In Vitro Metabolism Using Recombinant Enzymes. Pilot experiments demonstrated that CYP3A4 and CYP3A5 solithromycin metabolite formation, assessed by disappearance of solithromycin, was in the linear stage up to 10 and 60 minutes, respectively (Supplemental Fig. 4). Kinetic parameters could not be determined for CYP3A7, since no disappearance of solithromycin was detected up to 60 minutes for 1 μM and 10 μM solithromycin (Supplemental Fig. 4). Michaelis-Menten kinetic parameters for CYP3A4 and CYP3A5 are presented in Table 2 (Supplemental Figs. 5 and 6). For CYP3A5, the V_{max} could not adequately be assessed because of the high K_M and the influence of time-dependent inhibition at concentrations >30 μM (Supplemental Fig. 6; Table 2).

Adult Solithromycin PBPK Model Evaluation. The final model parameters for solithromycin, ketoconazole, and midazolam are shown in Table 1. The solithromycin PBPK model was evaluated using concentration versus time data from 100 healthy subjects and 22 patients with CABP (1966 plasma samples) from phase 1 and phase 2 studies (Fig. 1 and Supplemental Fig. 7) (Salerno et al., 2017). There were 50%, 60%, and 85% of simulated PK parameters (C_{max} and $AUC_{0\text{-}\tau}$) within 1.33-, 1.5-, and 2.0-fold of the observed values reported in adults (Table 3). There were 45%, 64%, and 91% of simulated CL or CL/F values within 1.33-, 1.5-, and 2.0-fold of the observed CL or CL/F values reported in adults (Supplemental Table 2). Finally, 89%, 56%, and 44% of the AFE values comparing observed and simulated concentrations across all adult and pediatric dosing regimens were within 2.0-fold, 1.5-fold, and 1.33-fold, respectively (Supplemental Table 3).

Adult Solithromycin DDI Predictions in Healthy Volunteers. The geometric mean ratio (90% confidence interval) for C_{max} and $AUC_{0\text{-}\infty}$ for oral midazolam (0.075 mg/kg) plus oral solithromycin (400 mg daily for 5 days or 800 mg day 1 followed by 400 mg daily for 4 days) relative to oral midazolam alone were similar between the simulations and the observed data collected from phase 1 studies in healthy adult volunteers (Table 4). Furthermore, the geometric mean ratio (90% confidence interval) for C_{max} and $AUC_{0\text{-}\infty}$ after a single dose of 400 mg oral solithromycin with 5 days of oral ketoconazole dosing relative to a single dose of 400 mg oral solithromycin alone were comparable between the simulations and the observed data (Table 4). In particular, all of the mean simulated versus observed fold ratios for C_{max} and $AUC_{0\text{-}\infty}$ were within 1.5-fold (Table 4).

Sensitivity Analysis. The most sensitive parameters for the steady-state half-life in a virtual adult receiving the oral regimen of solithromycin was the liver volume, the relative expression of CYP3A4 in liver, lipophilicity, CYP3A4 time-dependent inhibition and metabolism parameters (K_M, V_{max}, k_{inact}, K_I), and the CYP3A4 ontogeny factor and the CYP3A4 half-life in the liver.

Pediatric Solithromycin PBPK Model Evaluation. The simulated plasma concentrations in pediatric patients receiving intravenous solithromycin and oral suspension were slightly overpredicting the observed plasma concentrations and variability. The AFE comparing observed and simulated concentrations for the pediatric intravenous formulation, oral suspension, and oral capsules were 0.61, 0.83, and 0.56 (Figs. 2 and 3). Underprediction of the variability may be associated with differences in the virtual pediatric population within PK-Sim and the patient population with suspected or confirmed bacterial infection. The day 1 weight-normalized CL from the PBPK simulation were similar to the individual empirical Bayesian post hoc parameter estimates from the published PopPK model for all ages except 2 to <6 year old children (Supplemental Table 4) (Gonzalez et al., 2018).

Solithromycin Plus Midazolam DDI Simulations. The simulated age- and weight-based solithromycin intravenous doses (60-minute infusion) resulted in comparable solithromycin exposure but higher variability when compared with the mean ± S.D. $AUC_{0\text{-}24,ss}$ value (13 ± 4.38 mg*h/L) reported in healthy adults receiving 400 mg intravenously daily for 7 days (Fig. 4; Table 3). The simulated solithromycin $AUC_{0\text{-}24,ss}$ was generally the same across age groups, albeit slightly higher in pediatric patients to adults overall and highest and most variable in infants from 1 to <6 months and adolescents from 12 to <18 years of age (Fig. 4). The geometric mean $AUC_{0\text{-}\infty}$ ratio and associated 90%

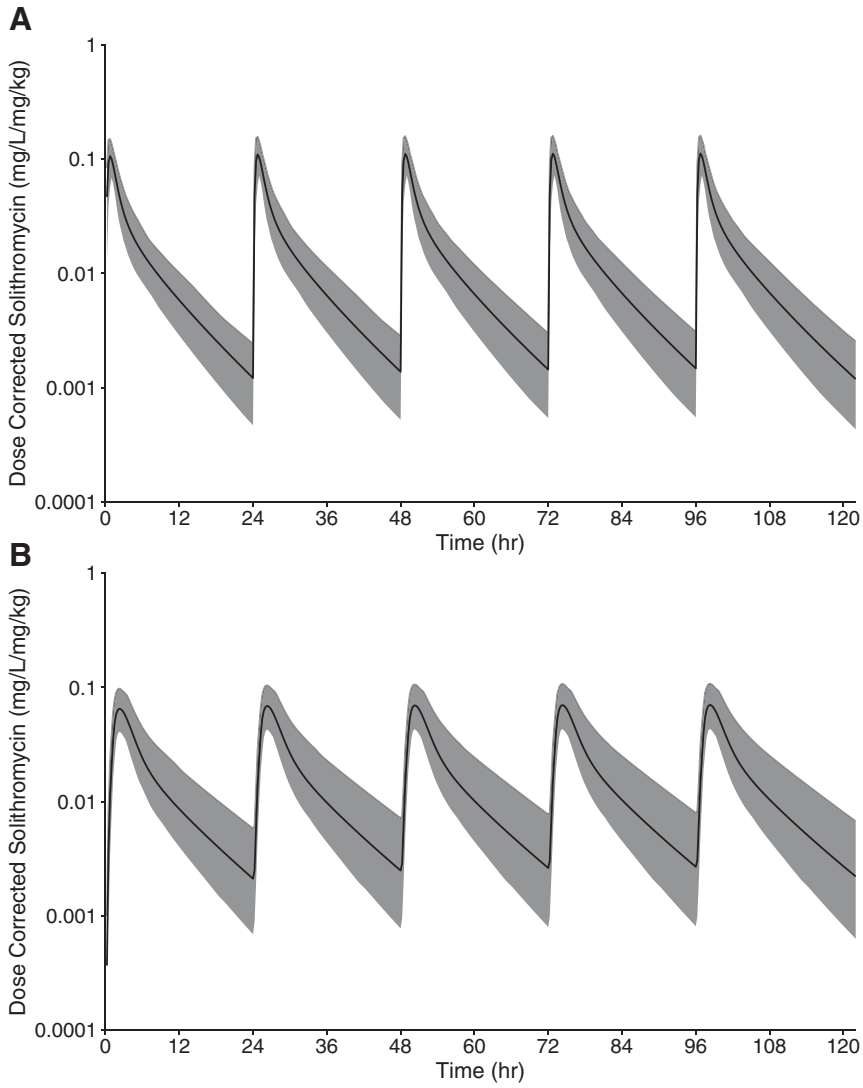

Fig. 3. Population simulations depicting concentration versus time in hours (hr) after the first dose of solithromycin oral administration (capsules or suspension) in pediatric patients. (A) Population simulations for 100 White American virtual infants and children from 4 days to 12 years of age receiving 1 mg/kg oral solithromycin as a suspension. (B) Population simulations for 100 White American virtual children and adolescents from 6 to 17 years of age receiving 1 mg/kg oral solithromycin as a capsule. The solid gray region is the 90% prediction interval, the solid black line is the simulated arithmetic mean, and the black dots are observed data from pediatric subjects. Solithromycin plasma concentration data were normalized by dose and time relative to the last drug administration since dose and administration differed for each individual.

confidence interval for midazolam with solithromycin relative to midazolam alone was slightly higher in simulated pediatric patients relative to simulated adults. Therefore, the proposed dose adjustment for midazolam, when given in combination with solithromycin, is approximately 9-fold lower in pediatric patients (Fig. 5; Table 5).

Solithromycin Plus Ketoconazole DDI Simulations. The simulated median ketoconazole $AUC_{0\text{-}24,ss}$ was generally the same across age groups using the recommended dosing, but the mean was higher in simulated infants from 1 to <6 months of age due to higher variability (Fig. 4). The geometric mean AUC_{∞} ratio and associated 90% confidence interval for solithromycin with ketoconazole relative to solithromycin alone was similar between virtual pediatric patients ≥6 months of age and adults, but higher in infants from 1 to <6 months of age. Therefore, the proposed dose adjustment for solithromycin when given in combination with ketoconazole is approximately 2-fold lower in infants <6 months of age and approximately 1.4-fold lower in ages ≥6 months (Fig. 5; Table 5).

Discussion

Although phenotyping studies for CYP3A4 are routinely performed for new investigational drugs, the role of CYP3A7 is rarely investigated, since CYP3A7 is minimally expressed in adults (https://www.fda.gov/regulatory-information/search-fda-guidance-documents/vitro-drug-interaction-studiescytochrome-p450-enzyme-and-transporter-mediated-drug-interactions) (https://www.fda.gov/regulatory-information/search-fda-guidancedocuments/clinical-drug-interaction-studies-cytochrome-p450-enzyme-and-transporter-mediated-druginteractions) (US Food and Drug Administration, 2020). However, CYP3A7 is the predominantly expressed CYP3A isoenzyme in fetal tissue and newborns, and CYP3A7 played a critical role in the CYP3A-mediated DDI between sildenafil plus fluconazole in neonates (Salerno et al., 2021). Therefore, the objective of this study was to leverage solithromycin as a case study to suggest a framework for investigating and incorporating CYP3A into adult and pediatric PBPK models to predict pediatric CYP3A mediated DDI potential during drug development. As demonstrated in this study, adult and pediatric PBPK models can be developed incorporating relevant CYP3A parameters, evaluated using adult and pediatric PK and adult DDI data, and then dosing can be simulated in pediatric patients receiving CYP3A drug combinations (Fig. 6). This approach can be applied to guide DDI assessment throughout drug development for other CYP3A drugs likely to be coadministered to pediatric patients.

We evaluated CYP3A4, CYP3A5, and CYP3A7 metabolism and time-dependent inhibition, and incorporated parameters for CYP3A4 and CYP3A5 into a published adult PBPK model for solithromycin

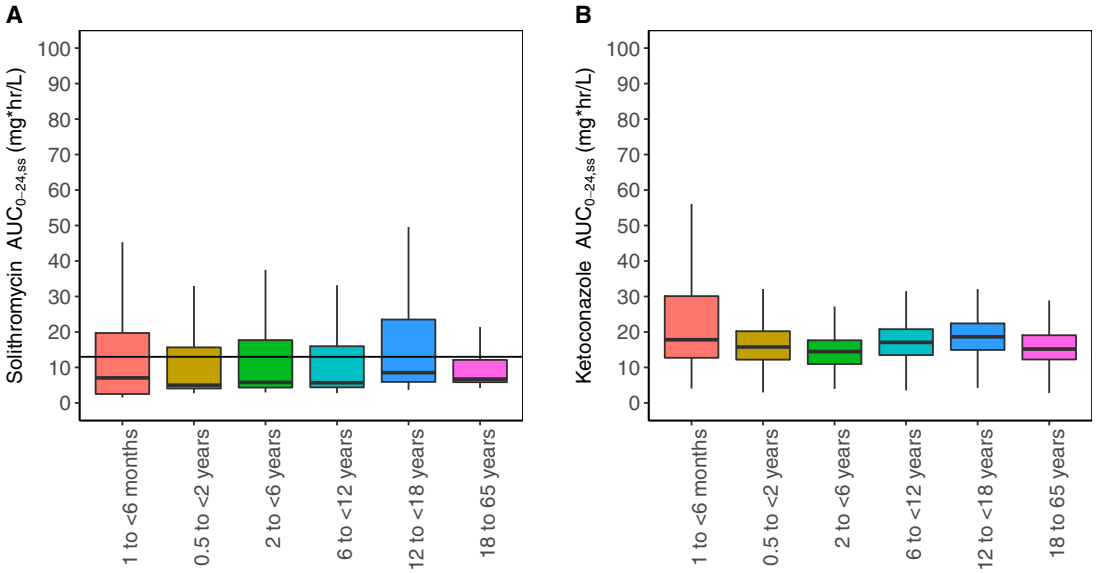

Fig. 4. Simulated solithromycin and ketoconazole daily steady-state area under the concentration versus time curve from 0 to 24 hours ($AUC_{0\text{-}24,ss}$) stratified by age group. Dosing was simulated in 500 virtual individuals between the ages of 1 and <6 months, 0.5 to <2 years, 2 to <6 years, 6 to <12 years, 12 to <18 years, and 18 to 65 years. The boxplots display the median (interquartile range), the upper whiskers are the 75th percentile to 1.5 times the interquartile range, the lower whisker is the 25th percentile subtract 1.5 times the interquartile range, and observations outside the whiskers are represented as black dots. (A) The simulated solithromycin daily $AUC_{0\text{-}24,ss}$ based on the age- and weight-based intravenous solithromycin dosing for 5 days as presented in Table 5. The red dot is the arithmetic mean for each age group. The black horizontal line refers to the mean daily $AUC_{0\text{-}24,ss}$ value observed in healthy adults whom received 400 mg intravenously for 7 days, in which the reported mean ± S.D. was 13 ± 4.38 mg*h/L (sponsor data on file). (B) The simulated ketoconazole daily $AUC_{0\text{-}24,ss}$ based on the age- and weight-based oral ketoconazole dosing for 5 days as presented in Table 5.

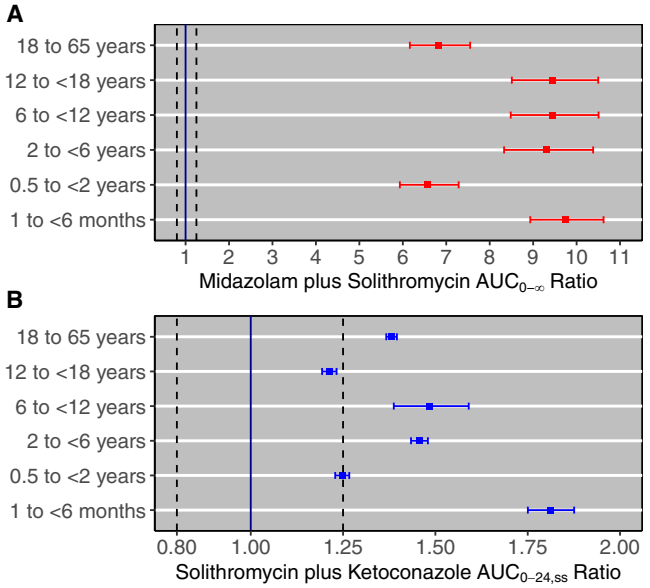

Fig. 5. Forest plots of the geometric mean fold ratios for the simulated AUC of midazolam with and without solithromycin and of solithromycin with and without ketoconazole, stratified by age groups. Dosing was simulated in 500 virtual individuals in each age category (1 to <6 months, 0.5 to <2 years, 2 to <6 years, 6 to <12 years, 12 to <18 years, and 18 to 65 years) according to the age- and weight-based dosing presented in Table 5. The vertical blue line corresponds to a ratio of 1.00 and the dotted vertical lines refer to the equivalence range of 0.80 to 1.25. (A) Virtual individuals received a single intravenous dose of midazolam alone and on the last date after 5 days of daily solithromycin intravenous dosing. The geometric mean ratio and 90% confidence interval of the $AUC_{0\text{-}\infty}$ was calculated for a group of virtual individuals receiving midazolam plus solithromycin relative to a group of virtual individuals receiving midazolam alone. (B) Virtual individuals received 5 days of solithromycin intravenous dosing alone as well as in combination with 5 days of oral ketoconazole dosing. The geometric mean ratio and 90% confidence interval of the $AUC_{0\text{-}24,ss}$ was calculated for the group of patients receiving solithromycin plus ketoconazole relative to a group receiving of virtual individuals solithromycin alone.

(Salerno et al., 2017). Using recombinant enzymes, we reported a higher k_{inact} and K_I for CYP3A4 than prior studies with human liver microsomes (0.084 minute^{-1} vs. 0.022 minute^{-1} and 0.34 μg/ml after protein binding correction vs. 0.038 μg/ml) (Salerno et al., 2017). There may be altered activity and expression between recombinant enzymes and human liver microsomes. In addition, we investigated solithromycin concentrations ≤300 μg/ml and used the NADPH regenerating system and testosterone as the probe substrate; whereas, the sponsor investigated solithromycin ≤0.3 μg/ml and used NADPH and midazolam as the probe substrate (sponsor data on file). Interestingly, solithromycin was not a substrate or time-dependent inhibitor for CYP3A7 at the concentrations (≤900 μg/ml) and times (60 minutes) investigated in this study. In contrast, CYP3A7 has been reported to have activity for midazolam, tacrolimus, clarithromycin, and alprazolam (Lacroix et al., 1997; Williams et al., 2002; Kamdem et al., 2005; Takahiro et al., 2015; Li and Lampe, 2019). Although substrate specificity can overlap for the CYP3A family, CYP3A7 generally has lower catalytic activity than CYP3A4 (Williams et al., 2002).

The solithromycin PBPK model included CYP3A4 and CYP3A5 metabolism and time-dependent inhibition, glomerular filtration, and P-glycoprotein transport and enterohepatic recirculation. The AFE of simulated versus observed concentrations and simulated PK parameters were all within 2-fold of observed values in healthy subjects and patients with CABP, except for the 200 mg, oral, administration day 1 C_{max} and the 600 mg, oral administration, daily day 7 AUC_{τ} (Supplemental Tables 2 and 3; Table 3). However, solithromycin regimens that demonstrated efficacy for CABP (800 mg on day 1 followed by 400 mg on days 2–5 orally and 400 mg intravenously daily) were well characterized (Barrera et al., 2016; File et al., 2016). In addition, simulated geometric mean ratios for midazolam with and without solithromycin and solithromycin with and without ketoconazole for C_{max} and AUC_{∞} were within 1.5-fold of values reported in healthy adults from phase II DDI studies (Table 4).

The adult solithromycin PBPK model was scaled to pediatric patients from 0 to 17 years of age. The weight-normalized day 1 CL for the

TABLE 5

Simulated dosing and DDI potential stratified by age group for solithromycin in combination with midazolam and ketoconazole.

Age Group	Solithromycin Simulated Dose[a]	Midazolam Simulated Dose	Ketoconazole Simulated Dose[b]	Midazolam plus Solithromycin $AUC_{0-\infty}$ Fold Change[c]	Solithromycin plus Ketoconazole $AUC_{0-24,ss}$ Fold Change[d]
1 to <6 months	3.25 mg/kg i.v.	0.05 mg/kg i.v.	3.3 mg/kg oral daily	9.7 (8.9, 10.6)	1.8 (1.8, 1.9)
1 to <6 months, no P-glycoprotein ontogeny function	3.25 mg/kg i.v.	0.05 mg/kg i.v.	3.3 mg/kg oral daily	9.7 (8.9, 10.5)	1.8 (1.7, 2.0)
0.5 to <2 years	6 mg/kg i.v.	0.05 mg/kg i.v.	4 mg/kg oral daily	6.6 (5.9, 7.3)	1.2 (1.2, 1.3)
0.5 to <2 years, no P-glycoprotein ontogeny function	6 mg/kg i.v.	0.05 mg/kg i.v.	4 mg/kg oral daily	6.6 (5.9, 7.3)	1.2 (1.2, 1.3)
2 to <6 years	7 mg/kg i.v.	0.05 mg/kg i.v.	3.3 mg/kg oral daily	9.3 (8.3, 10.4)	1.5 (1.4, 1.5)
2 to <6 years, no P-glycoprotein ontogeny function	7 mg/kg i.v.	0.05 mg/kg i.v.	3.3 mg/kg oral daily	9.3 (8.3, 10.4)	1.5 (1.4, 1.6)
6 to <12 years	6 mg/kg i.v.	0.025 mg/kg i.v.	3.3 mg/kg oral daily	9.4 (8.5, 10.5)	1.5 (1.4, 1.6)
12 to <18 years	5.5 mg/kg i.v.	0.5 mg i.v.	3.3 mg/kg oral daily	9.5 (8.5, 10.5)	1.2 (1.2, 1.2)
18–65 years	400 mg i.v.	0.5 mg i.v.	200 mg oral daily	6.8 (6.2, 7.6)	1.4 (1.4, 1.4)

[a]The maximum simulated solithromycin dose was 400 mg.
[b]The maximum simulated ketoconazole dose was 200 mg.
[c]The fold-change values are presented as the geometric mean (90% confidence interval) for midazolam based on 500 simulations in each age group receiving midazolam plus solithromycin for 5 days relative to midazolam alone for 5 days.
[d]The fold-change values are presented as the geometric mean (90% confidence interval) for solithromycin based on 500 simulations in each age group receiving solithromycin plus ketoconazole for 5 days relative to solithromycin alone for 5 days.
Abbreviations: intravenous: i.v.

PBPK simulations were similar to the individual empirical Bayesian post hoc parameter estimates from a published PopPK model developed using data for these children (Supplemental Table 4) (Gonzalez et al., 2018). However, our steady-state CL and simulated age- and weight-based dosing for intravenous solithromycin were lower than the PopPK model recommendations (8 mg/kg intravenously daily) (Table 5) (Gonzalez et al., 2018). The final PopPK model included weight and a sigmoidal maturation function for PMA on CL, but time-dependent inhibition was not included (Gonzalez et al., 2018). The differences in steady-state CL and suggested dosing between the PopPK and PBPK models are primarily due to the inclusion of time-dependent inhibition in our PBPK model.

To evaluate CYP3A mediated DDI potential for solithromycin, adult and pediatric PBPK models were developed for the CYP3A probe substrate, midazolam, as well as the strong CYP3A inhibitor, ketoconazole. After scaling the adult oral ketoconazole PBPK model to pediatric patients, the plasma concentrations were overpredicted (Supplemental Material). Oral absorption of ketoconazole is highly affected by the presence of food in the gastrointestinal tract and by gastric acidity, which may differ in children with candidiasis relative to healthy adults (Van Tyle, 1984). The intragastric pH is elevated in neonates, and a study in neonates reported that gastric pH above 2.5 and continuous oral feeding resulted in insufficient ketoconazole absorption in preterm infants during the first week of life (Van Den Anker et al., 1994; Kearns et al., 2003). Formulation also plays a role as children (2 to 12.5 years of age) receiving ketoconazole suspension had mean plasma concentrations 1.6 to 4 times higher than children receiving crushed tablets in applesauce (Ginsburg et al., 1983). After reducing the transcellular intestinal permeability, simulated exposures were similar to observed data in children with candidiasis. Of note, the optimized transcellular intestinal permeability for ketoconazole is significantly greater than the predicted value ($2.39 * 10^{-6}$ cm/min) in PK-Sim based on its physiochemical properties. It is likely that the aqueous solubility of ketoconazole is significantly improved when formulated with the excipients in the tablet, which might in part explain this discrepancy. Ketoconazole has not been systematically studied in children under 2 years of age, so dosing was simulated to achieve similar AUC_τ relative to adults receiving 200-mg tablets oral daily as well as children ≥2 years of age receiving 3.3 mg/kg per day ketoconazole (Fig. 4; Table 5). Consistent with allometric principles, our simulations suggest that a slightly higher weight-based dosage (4 mg/kg per day) should be given to young children between 0.5 and 2 years of age (Anderson and Holford, 2013).

Interestingly, the differences in DDI potential simulated across age cohorts for midazolam plus solithromycin and solithromycin plus ketoconazole reflect differences in inhibitor concentrations (Figs. 4 and 5). For example, due to the high variability in solithromycin and ketoconazole concentrations between 1 and <6 months of age, exposures were highest and resulted in the highest AUC ratios with and without inhibition in this age group. This study suggests that, as long as the inhibitor concentrations are closely matched to adult concentrations, DDI potential for drug primarily metabolized through CYP3A4 should be similar between pediatric subjects >1 month of age and adults. However, the exposure-response relationship and drug concentrations can differ between pediatric and adult patients due to differences in disease progression and treatment response, such as for drugs involved in the treatment of gastroesophageal reflux disorder in infancy, neonatal bacterial conjunctivitis, type 2 diabetes, oncology products, major depression disorder, as well as attention-deficit hyperactivity disorder (Sun et al., 2018). Additionally, DDI potential may differ in neonates for other CYP3A substrates metabolized by CYP3A7, since CYP3A7 has greater expression in neonates and generally has lower catalytic activity than CYP3A4.

In conclusion, we present a framework for incorporating CYP3A parameters to predict pediatric CYP3A mediated DDI potential during drug development. However, there are some notable limitations that warrant further discussion. First, we were unable to determine the true V_{max} for CYP3A5 because of the high K_M and the influence of time-dependent inhibition at higher solithromycin concentrations. Solithromycin steady-state half-life was not sensitive to CYP3A5, which can also be expected due to the high K_M value. Second, the lack of significant metabolism of solithromycin by CYP3A7 made it difficult to evaluate the role of CYP3A7 in CYP3A mediated DDI potential in neonates. Since we cannot predict in advance whether a drug will be a CYP3A7 substrate, CYP3A7 metabolism should still be explored if the investigational drug is likely to be given to infants. Another limitation is with respect to the ontogeny function for P-glycoprotein. We evaluated

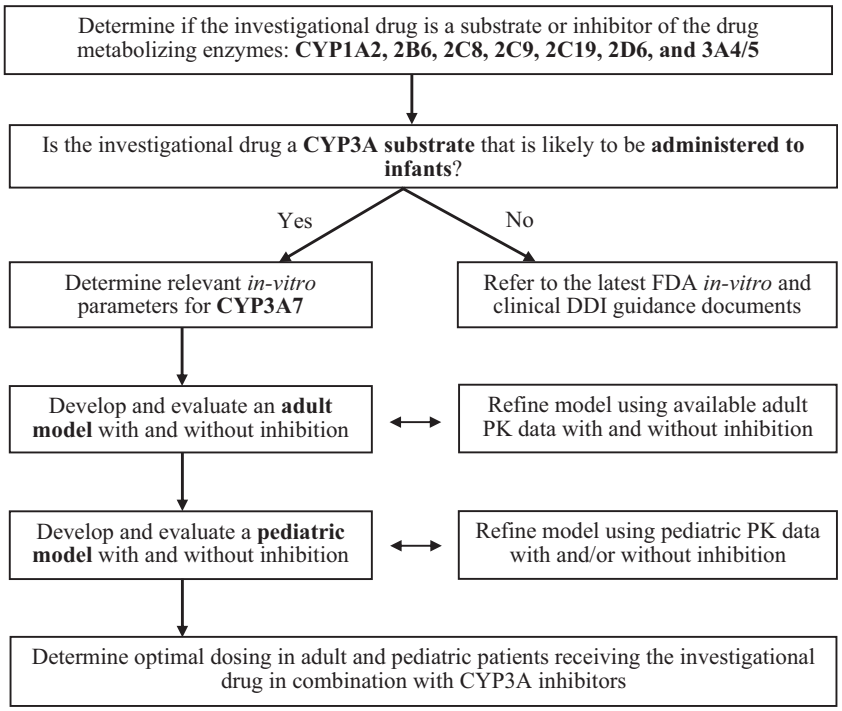

Fig. 6. Approach for leveraging experimental data and PBPK modeling to predict DDIs mediated via CYP3A inhibition in adults and pediatric patients during drug development. We have proposed a framework for conducting and integrating relevant experimental studies into adult and pediatric PBPK models to predict pediatric CYP3A mediated DDI potential during drug development. Although in vitro studies for CYP3A4 and CYP3A5 are routinely performed to evaluate metabolism and drug interaction potential for new investigational drugs, in vitro studies for CYP3A7 are rarely performed since CYP3A7 is minimally expressed in adults (https://www.fda.gov/regulatory-information/search-fdaguidance-documents/vitro-drug-interaction-studies-cytochrome-p450-enzyme-and-transportermediated-drug-interactions; https://www.fda.gov/regulatory-information/search-fda-guidance-documents/clinical-drug-interaction-studies-cytochrome-p450-enzyme-and-transporter-mediated-drug-interactions). However, CYP3A7 is the predominantly expressed CYP3A isoenzyme in fetal tissue and newborns, and we have previously demonstrated that CYP3A7 was integral for evaluating CYP3A mediated DDIs in infants <2 months of age using the CYP3A substrate, sildenafil, as an example (Salerno et al., 2021). Therefore, we recommend determining whether a drug is a substrate and/or inhibitor of CYP3A7 if this drug is likely to be administered concurrently to infants with other CYP3A inhibitors/inducers or CYP3A7 substrates, respectively. These in vitro parameters can be incorporated into an adult PBPK model developed and evaluated using clinical PK data and DDI data collected in healthy adults. The adult DDI PBPK model can be scaled to pediatric patients and evaluated using available pediatric PK data with and/or without drug inhibition. We recommend extensively evaluating the victim and perpetrator pediatric PBPK models using pediatric PK data for the drugs administered separately prior to comodeling and simulated the DDI in pediatric patients. Finally, dosing recommendations with and without drug inhibitors can be simulated across the pediatric age continuum and provided within the product labeling. The advantage of this approach is that it does not require pediatric clinical DDI data since such studies are rarely performed unless children receive the drug combinations per standard of care. However, as clinical data becomes available in pediatric patients receiving the drug combinations per standard of care, the dosing recommendations can be further refined using opportunistic PK data.

the DDI simulations with and without incorporation of an ontogeny function for P-glycoprotein expression with a mean ± S.D. age at which 50% of adult expression is reached at 2.94 ± 1.33 years (Prasad et al., 2016). This ontogeny function is based upon P-glycoprotein protein fragment quantification data in pediatric and adult liver tissues and may not be a true indication of P-glycoprotein function. Furthermore, the CYP3A ontogeny function implemented in the simulations may also influence the results as one study reported that the predicted ivabradine and metabolite AUC with ketoconazole relative to control were 2-fold lower and 1.3-fold higher in the youngest children (0.5–1 year old) compared with adults using ontogeny functions derived by Salem, et al. (2014) and Upreti, et al. (2016), respectively (Lang et al., 2020). However, the CYP3A ontogeny functions used in this study captured the observed DDI in preterm infants receiving sildenafil plus fluconazole (Salerno et al., 2021). Finally, the simulated solithromycin age- and weight-based dosing differed from the recommended dosing of 8 mg intravenously daily that was investigated for safety in pediatric studies primarily because time-dependent inhibition was not included in the PopPK model. Additionally, there are likely disease-state differences in the pediatric population that are not accounted for in the virtual pediatric population.

Authorship Contributions

Participated in research design: Salerno, Gonzalez.

Conducted experiments: Salerno.

Performed data analysis: Salerno, Carreño.

Wrote or contributed to the writing of the manuscript: Salerno, Carreño, Edginton, Cohen-Wolkowiez, Gonzalez.

References

Anderson BJ and Holford NHG (2013) Understanding dosing: Children are small adults, neonates are immature children. *Arch Dis Child* **98**:737–744.

Van Den Anker J, Van Ussel-Dijk A, and Woestenborghs R (1994) Abstract 9: The effect of gastric pH on the absorption of ketoconazole by very-low-birth weight infants. *Pediatr Res* **36**:4.

Barrera CM, Mykietiuk A, Metev H, Nitu MF, Karimjee N, Doreski PA, Mitha I, Tanaseanu CM, Molina JM, Antonovsky Y, et al.; SOLITAIRE-ORAL Pneumonia Team (2016) Efficacy and safety of oral solithromycin versus oral moxifloxacin for treatment of community-acquired bacterial pneumonia: a global, double-blind, multicentre, randomised, active-controlled, non-inferiority trial (SOLITAIRE-ORAL). *Lancet Infect Dis* **16**:421–430.

Berezhkovskiy LM (2004) Determination of volume of distribution at steady state with complete consideration of the kinetics of protein and tissue binding in linear pharmacokinetics. *J Pharm Sci* **93**:364–374.

Bourcier K, Hyland R, Kempshall S, Jones R, Maximilien J, Irvine N, and Jones B (2010) Investigation into UDP-glucuronosyltransferase (UGT) enzyme kinetics of imidazole- and triazole-containing antifungal drugs in human liver microsomes and recombinant UGT enzymes. *Drug Metab Dispos* **38**:923–929.

Buege MJ, Brown JE, and Aitken SL (2017) Solithromycin: A novel ketolide antibiotic. *Am J Health Syst Pharm* **74**:875–887.

Burchell B, Coughtrie M, Jackson M, Harding D, Fournel-Gigleux S, Leakey J, and Hume R (1989) Development of human liver UDP-glucuronosyltransferases. *Dev Pharmacol Ther* **13**:70–77.

DrugBank.DrugBank 5.0 (2018) < https://go.drugbank.com/> Accessed Jan 01, 2021.

File Jr TM, Rewerska B, Vucinić-Mihailović V, Gonong Jr JRV, Das AF, Keedy K, Taylor D, Sheets A, Fernandes P, Oldach D et al.; SOLITAIRE-IV Pneumonia Team (2016)

SOLITAIRE-IV: A randomized, double-blind, multicenter study comparing the efficacy and safety of intravenous-to-oral solithromycin to intravenous-to-oral moxifloxacin for treatment of community-acquired bacterial pneumonia. *Clin Infect Dis* **63**:1007–1016.
Gibbs MA, Thummel KE, Shen DD, and Kunze KL (1999) Inhibition of cytochrome P-450 3A (CYP3A) in human intestinal and liver microsomes: comparison of Ki values and impact of CYP3A5 expression. *Drug Metab Dispos* **27**:180–187.
Ginsburg CM, McCracken Jr GH, and Olsen K (1983) Pharmacology of ketoconazole suspension in infants and children. *Antimicrob Agents Chemother* **23**:787–789.
Gonzalez D, James LP, Al-Uzri A, Bosheva M, Adler-Shohet FC, Mendley SR, Bradley JS, Espinosa C, Tsonkova E, Moffett K et al. (2018) Population pharmacokinetics and safety of solithromycin following intravenous and oral administration in infants, children, and adolescents. *Antimicrob Agents Chemother* **62**:62.
Gonzalez D, Palazzi DL, Bhattacharya-Mithal L, Al-Uzri A, James LP, Bradley J, Neu N, Jasion T, Hornik CP, Smith PB et al. (2016) Solithromycin pharmacokinetics in plasma and dried blood spots and safety in adolescents. *Antimicrob Agents Chemother* **60**: 2572–2576.
Grimm SW, Einolf HJ, Hall SD, He K, Lim H-K, Ling K-HJ, Lu C, Nomeir AA, Seibert E, Skordos KW et al. (2009) The conduct of in vitro studies to address time-dependent inhibition of drug-metabolizing enzymes: a perspective of the pharmaceutical research and manufacturers of America. *Drug Metab Dispos* **37**:1355–1370.
Grimstein M, Yang Y, Zhang X, Grillo J, Huang SM, Zineh I, and Wang Y (2019) Physiologically based pharmacokinetic modeling in regulatory science: An update from the U.S. Food and Drug Administration's office of clinical pharmacology. *J Pharm Sci* **108**:21–25.
Hallifax D and Houston JB(2006) Letter to the editor: Binding of drugs to hepatic microsomes: Comment and assessment of current prediction methodology with recommendation for improvement. *Drug Metab Dispos* **34**:724–727.
Harwood MD, Neuhoff S, Carlson GL, Warhurst G, and Rostami-Hodjegan A (2013) Absolute abundance and function of intestinal drug transporters: a prerequisite for fully mechanistic in vitro-in vivo extrapolation of oral drug absorption. *Biopharm Drug Dispos* **34**:2–28.
Hyland R, Jones BC, and Smith DA (2003) Identification of the cytochrome P450 enzymes involved in the N-oxidation of voriconazole. *Drug Metab Dispos* **31**:540–547.
Janssen Pharmaceuticals Nizoral Ketoconazole Tablets. <https://www.accessdata.fda.gov/drugsatfda_docs/label/2013/018533s040lbl.pdf> Accessed Jan 01, 2021.
Jiang X-L, Zhao P, Barrett JS, Lesko LJ, and Schmidt S (2013) Application of physiologically based pharmacokinetic modeling to predict acetaminophen metabolism and pharmacokinetics in children. *CPT Pharmacometrics Syst Pharmacol* **2**:e80.
Johnson TN, Tanner MS, Taylor CJ, and Tucker GT (2001) Enterocytic CYP3A4 in a paediatric population: developmental changes and the effect of coeliac disease and cystic fibrosis. *Br J Clin Pharmacol* **51**:451–460.
Johnson TN, Zhou D, and Bui KH (2014) Development of physiologically based pharmacokinetic model to evaluate the relative systemic exposure to quetiapine after administration of IR and XR formulations to adults, children and adolescents. *Biopharm Drug Dispos* **35**:341–352.
Kamdem LK, Streit F, Zanger UM, Brockmöller J, Oellerich M, Armstrong VW, and Wojnowski L (2005) Contribution of CYP3A5 to the in vitro hepatic clearance of tacrolimus. *Clin Chem* **51**:1374–1381.
Kearns GL, Abdel-Rahman SM, Alander SW, Blowey DL, Leeder JS, and Kauffman RE (2003) Developmental pharmacology–drug disposition, action, and therapy in infants and children. *N Engl J Med* **349**:1157–1167.
Lacroix D, Sonnier M, Moncion A, Cheron G, and Cresteil T (1997) Expression of CYP3A in the human liver–evidence that the shift between CYP3A7 and CYP3A4 occurs immediately after birth. *Eur J Biochem* **247**:625–634.
Lang J, Vincent L, Chenel M, Ogungbenro K, and Galetin A (2020) Impact of Hepatic CYP3A4 ontogeny functions on drug–drug interaction risk in pediatric physiologically-based pharmacokinetic/pharmacodynamic modeling: Critical literature review and ivabradine case study. *Clin Pharmacol Ther*; Epub Ahead of Print.
Lexicomp Online (2020) Lexicomp Drug Information. <https://online.lexi.com/lco/action/login?reauth> Accessed Jan 01, 2021.
Li H and Lampe JN (2019) Neonatal cytochrome P450 CYP3A7: A comprehensive review of its role in development, disease, and xenobiotic metabolism. *Arch Biochem Biophys* **673**:108078.
MacLauchlin C, Schneider SE, Keedy K, Fernandes P, and Jamieson BD (2018) Metabolism, excretion, and mass balance of solithromycin in Humans. *Antimicrob Agents Chemother* **62**:e01474–e17.
Meyer M, Schneckener S, Ludewig B, Kuepfer L, and Lippert J (2012) Using expression data for quantification of active processes in physiologically based pharmacokinetic modeling. *Drug Metab Dispos* **40**:892–901.
Oishi M, Takano Y, Torita Y, Malhotra B, and Chiba K (2018) Physiological based pharmacokinetic modeling to estimate in vivo Ki of ketoconazole on renal P-gp using human drug-drug interaction study result of fesoterodine and ketoconazole. *Drug Metab Pharmacokinet* **33**:90–95.
Onishi S, Kawade N, Itoh S, Isobe K, and Sugiyama S (1979) Postnatal development of uridine diphosphate glucuronyltransferase activity towards bilirubin and 2-aminophenol in human liver. *Biochem J* **184**:705–707.
Pachot JI, Botham RP, Haegele KD, and Hwang K (2003) Experimental estimation of the role of P-Glycoprotein in the pharmacokinetic behaviour of telithromycin, a novel ketolide, in comparison with roxithromycin and other macrolides using the Caco-2 cell model. *J Pharm Pharm Sci* **6**:1–12.
PK-Sim (2017) PK-Sim Ontogeny Database. **Version 7.**:1–47.
Prasad B, Gaedigk A, Vrana M, Gaedigk R, Leeder JS, Salphati L, Chu X, Xiao G, Hop C, Evers R, et al. (2016) Ontogeny of hepatic drug transporters as quantified by LC-MS/MS proteomics. *Clin Pharmacol Ther* **100**:362–370.
Rodrigues AD (1999) Integrated cytochrome P450 reaction phenotyping: attempting to bridge the gap between cDNA-expressed cytochromes P450 and native human liver microsomes. *Biochem Pharmacol* **57**:465–480.
Salem F, Johnson TN, Abduljalil K, Tucker GT, and Rostami-Hodjegan A (2014) A re-evaluation and validation of ontogeny functions for cytochrome P450 1A2 and 3A4 based on in vivo data. *Clin Pharmacokinet* **53**:625–636.
Salem F, Rostami-Hodjegan A, and Johnson TN (2013) Do children have the same vulnerability to metabolic drug–drug interactions as adults? A critical analysis of the literature. *J Clin Pharmacol* **53**:559–566.
Salerno SN, Edginton A, Cohen-Wolkowiez M, Hornik CP, Watt KM, Jamieson BD, and Gonzalez D (2017) Development of an adult physiologically based pharmacokinetic model of solithromycin in plasma and epithelial lining fluid. *CPT Pharmacometrics Syst Pharmacol* **6**:814–822.
Salerno SN, Edginton A, Gerhart JG, Laughon MM, Ambalavanan N, Sokol GM, Hornik CD, Stewart D, Mills M, Martz K, et al.; Pharmaceuticals for Children Act - Pediatric Trials Network Steering Committee (2021) Physiologically-based pharmacokinetic modeling characterizes the CYP3A-mediated drug-drug interaction between fluconazole and sildenafil in infants. *Clin Pharmacol Ther* **109**:253–262.
Stevens JC, Hines RN, Gu C, Koukouritaki SB, Manro JR, Tandler PJ, and Zaya MJ (2003) Developmental expression of the major human hepatic CYP3A enzymes. *J Pharmacol Exp Ther* **307**:573–582.
Sun H, Temeck JW, Chambers W, Perkins G, Bonnel R, and Murphy D (2018) Extrapolation of efficacy in pediatric drug development and evidence-based medicine: Progress and lessons learned. *Ther Innov Regul Sci* **52**:199–205.
Takahiro R, Nakamura S, Kohno H, Yoshimura N, Nakamura T, Ozawa S, Hirono K, Ichida F, and Taguchi M (2015) Contribution of CYP3A isoforms to dealkylation of PDE5 inhibitors: a comparison between sildenafil N-demethylation and tadalafil demethylenation. *Biol Pharm Bull* **38**:58–65.
Tréluyer JM, Bowers G, Cazali N, Sonnier M, Rey E, Pons G, and Cresteil T (2003) Oxidative metabolism of amprenavir in the human liver. Effect of the CYP3A maturation. *Drug Metab Dispos* **31**:275–281.
US Food and Drug Administration (FDA) (2020). In vitro metabolism and transporter-mediated drug-drug interaction studies guidance for industry. <https://www.fda.gov/regulatory-information/search-fda-guidance-documents/vitro-drug-interaction-studies-cytochrome-p450-enzyme-and-transporter-mediated-drug-interactions> Accessed Jan 01, 2021.
Upreti VV and Wahlstrom JL (2016) Meta-analysis of hepatic cytochrome P450 ontogeny to underwrite the prediction of pediatric pharmacokinetics using physiologically based pharmacokinetic modeling. *J Clin Pharmacol* **56**:266–283.
Van Tyle JH (1984) Ketoconazole mechanism of action, spectrum of activity, drug interactions, adverse reactions and therapeutic use. *Pharmacotherapy* **4**:343–373.
von Moltke LL, Greenblatt DJ, Schmider J, Duan SX, Wright CE, Harmatz JS, and Shader RI (1996) Midazolam hydroxylation by human liver microsomes in vitro: inhibition by fluoxetine, norfluoxetine, and by azole antifungal agents. *J Clin Pharmacol* **36**:783–791.
Williams JA, Ring BJ, Cantrell VE, Jones DR, Eckstein J, Ruterbories K, Hamman MA, Hall SD, and Wrighton SA (2002) Comparative metabolic capabilities of CYP3A4, CYP3A5, and CYP3A7. *Drug Metab Dispos* **30**:883–891.
Xiao K, Gao J, Weng SJ, Fang Y, Gao N, Wen Q, Jin H, and Qiao HL (2019) CYP3A4/5 activity probed with testosterone and midazolam: Correlation between two substrates at the microsomal and enzyme levels. *Mol Pharm* **16**:382–392.
Zhang X, Yang Y, Grimstein M, Fan J, Grillo JA, Huang SM, Zhu H, and Wang Y (2020) Application of PBPK modeling and simulation for regulatory decision making and its impact on US prescribing information: An Update on the 2018-2019 submissions to the US FDA's office of clinical pharmacology. *J Clin Pharmacol* **60** (Suppl 1):S160–S178.
Zhou W, Johnson TN, Xu H, Cheung S, Bui KH, Li J, Al-Huniti N, and Zhou D (2016) Predictive performance of physiologically based pharmacokinetic and population pharmacokinetic modeling of renally cleared drugs in children. *CPT Pharmacometrics Syst Pharmacol* **5**:475–483.

Address correspondence to: Daniel Gonzalez, UNC Eshelman School of Pharmacy, The University of North Carolina at Chapel Hill, 301 Pharmacy Lane, Campus Box #7569, Chapel Hill, NC 27599-7569. E-mail: daniel.gonzalez@unc.edu

Supplementary Materials

DMD-AR-2020-000318R2

Leveraging Physiologically-Based Pharmacokinetic (PBPK) Modeling and Experimental Data to Guide Dosing Modification of CYP3A-Mediated Drug-Drug Interactions (DDIs) in the Pediatric Population

Sara N. Salerno, Fernando O. Carreño, Andrea N. Edginton, Michael Cohen-Wolkowiez, and Daniel Gonzalez

Division of Pharmacotherapy and Experimental Therapeutics, UNC Eshelman School of Pharmacy, The University of North Carolina at Chapel Hill, Chapel Hill, NC, USA (S.N.S., F.O.C., D.G.); School of Pharmacy, University of Waterloo, Kitchener, ON, Canada (A.N.E.); Duke Clinical Research Institute, Durham, NC, USA (M.C.W.); Department of Pediatrics, Duke University School of Medicine, Durham, NC, USA (M.C.W.).

Supplementary Methods

PK-Sim® Basic Model Structure

The generic model structure implemented within PK-Sim® includes the following 15 organs/tissues and blood pool compartments: adipose tissue, brain, bone, gonads, heart, kidneys, large intestine, small intestine, liver, lung, muscle, pancreas, skin, spleen, stomach, arterial blood, venous blood, and portal vein blood. The alimentary canal from the stomach to the rectum is divided into 12 compartments and a mucosal compartment was added to each luminal segment of the intestine (Thelen *et al.*, 2011). Each organ/tissue can further be described by the following sub-compartments: blood cells, interstitial space, intracellular space, and plasma. The portal vein, arterial blood, and venous blood compartments contain blood cells and plasma.

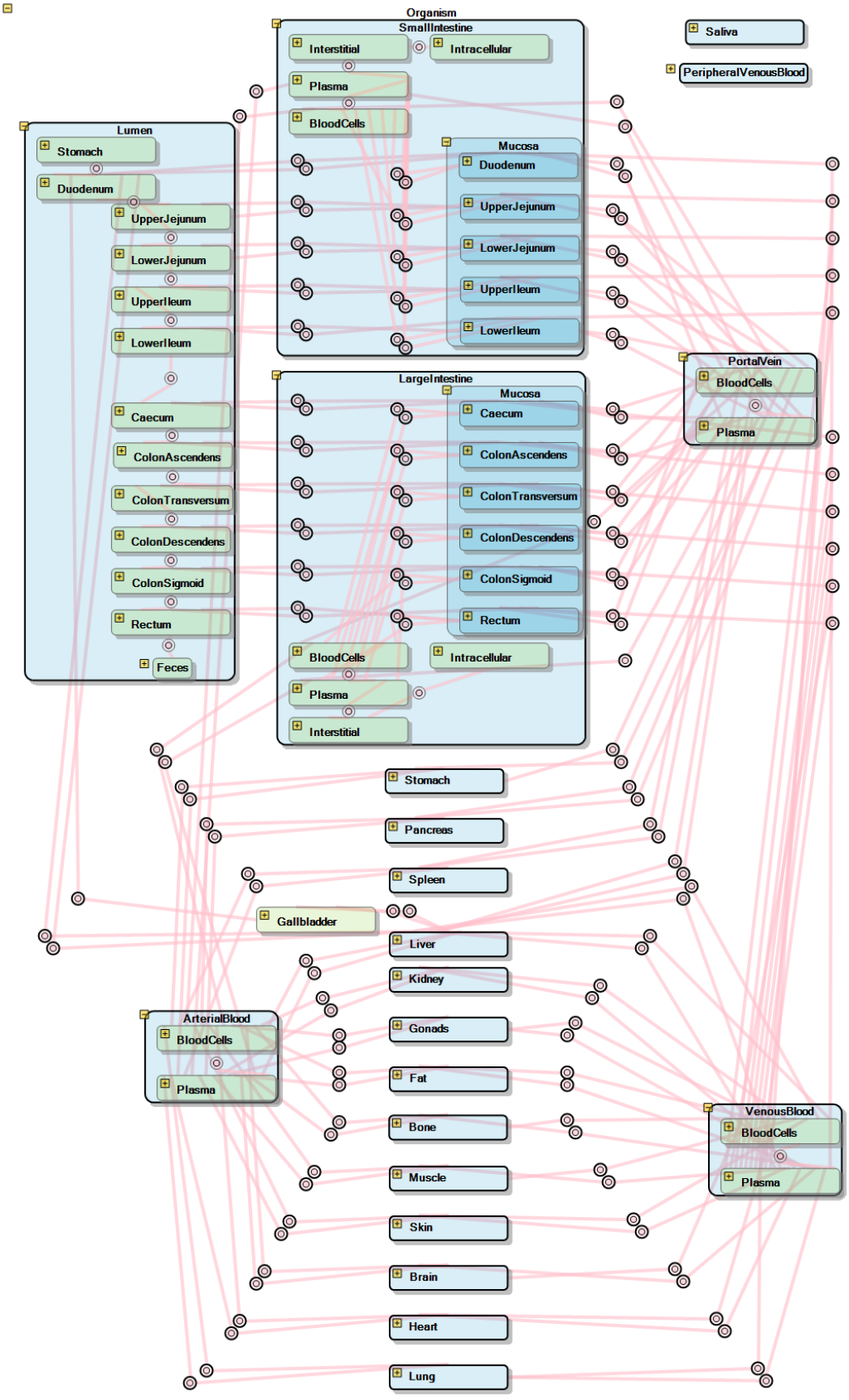
Organism
SmallIntestine
Interstitial
Intracellular
Plasma
BloodCells
Mucosa
Duodenum
UpperJejunum
LowerJejunum
UpperIleum
LowerIleum
Saliva
PeripheralVenousBlood
Lumen
Stomach
Duodenum
UpperJejunum
LowerJejunum
UpperIleum
LowerIleum
Caecum
ColonAscendens
ColonTransversum
ColonDescendens
ColonSigmoid
Rectum
Feces
LargeIntestine
Mucosa
Caecum
ColonAscendens
ColonTransversum
ColonDescendens
ColonSigmoid
Rectum
BloodCells
Intracellular
Plasma
Interstitial
PortalVein
BloodCells
Plasma
Stomach
Pancreas
Spleen
Gallbladder
Liver
Kidney
Gonads
Fat
Bone
Muscle
Skin
Brain
Heart
Lung
ArterialBlood
BloodCells
Plasma
VenousBlood
BloodCells
Plasma

Expression Database

PK-Sim® uses gene expression data to estimate tissue specific protein abundances and to determine catalytic rate constants for relevant enzymes or transporters affecting drug distribution. Relative protein abundance can be set according to available expression data while catalytic parameters are described by a global kinetic rate constant. The PK-Sim® library includes large-scale gene-expression data from publicly available sources, which were downloaded, processed, stored and customized such that they can be directly utilized in PBPK model building (Meyer *et al.*, 2012). This method enables direct estimation of *in vivo* enzyme and transporter activity based on data-based inclusion of tissue-specific protein abundance and significantly reduces the number of free model parameters needed. A summary of the expression data relevant within this manuscript is described below, and the full human gene expression database is found at: https://github.com/Open-Systems-Pharmacology/Suite/releases/tag/v9.1.

CYP3A4 Expression

	Unit ▲	Database ▼	
	Array	EST	RT-PCR
PK-Sim Or... ▲	E-GEOD-2361	UNIGENE	NISHIMURA et al...
Bone	1.378797		
Brain	1.061975	0.144231	0.507143
Cecum		8.333362	
Colon Ascendens	1.928030	8.333362	
Colon Descenden...	1.928030	8.333362	
Colon Sigmoid / D...	1.928030	8.333362	
Colon Transversum	1.928030	8.333362	
Duodenum	11.610519	4.687856	8.853683
Gonads	0.932457		0.095741
Heart	1.043729		
Kidney	1.059173	0.336227	0.652177
Large Intestine	1.928030	8.333362	
Liver Pericentral	29.034842	11.704407	121.667043
Liver Periportal	29.034842	11.704407	121.667043
Lower Ileum	11.610519	4.687856	8.853683
Lower Jejunum	11.610519	4.687856	8.853683
Lung	1.066114		0.051947
Muscle	0.911096	0.093647	
Pancreas	0.528164		
Rectum		8.333362	
Skin	1.149605		
Small Intestine	11.610519	4.687856	8.853683
Spleen	1.014539		
Stomach	1.275224	4.138795	
Upper Ileum	11.610519	4.687856	8.853683
Upper Jejunum	11.610519	4.687856	8.853683

CYP3A5 Expression

PK-Sim Or...	Unit: Array / Database: E-GEOD-2361	Unit: EST / Database: UNIGENE	Unit: RT-PCR / Database: NISHIMURA et al...
Bone	0.143476		
Brain	0.372156	0.194568	0.045975
Cecum		20.977490	
Colon Ascendens	3.225719	20.977490	
Colon Descenden...	3.225719	20.977490	
Colon Sigmoid / D...	3.225719	20.977490	
Colon Transversum	3.225719	20.977490	
Duodenum	12.014190	18.556920	5.915094
Gonads	0.487523	0.738123	
Heart	0.340563		
Kidney	1.205632	4.646800	1.848467
Large Intestine	3.225719	20.977490	
Liver Pericentral	9.675079	3.514307	10.996009
Liver Periportal	9.675079	3.514307	10.996009
Lower Ileum	12.014190	18.556920	5.915094
Lower Jejunum	12.014190	18.556920	5.915094
Lung	1.183043	4.146770	1.782112
Muscle	0.242893	0.280941	
Pancreas	0.777999	0.191018	
Rectum		20.977490	
Skin	2.120271		
Small Intestine	12.014190	18.556920	5.915094
Spleen	0.346684		
Stomach	9.492960	10.097364	
Upper Ileum	12.014190	18.556920	5.915094
Upper Jejunum	12.014190	18.556920	5.915094

AADAC Expression

	Unit ▲	Database ▲	
	Array	EST	RT-PCR
PK-Sim Or... ▲	E-GEOD-2361	UNIGENE	NISHIMURA et al...
Blood Cells			0.000578
Bone	0.374124		0.000720
Brain	0.247552		0.000588
Cecum		3.616065	
Colon Ascendens	0.246923	3.616065	0.001536
Colon Descenden...	0.246923	3.616065	0.001536
Colon Sigmoid / D...	0.246923	3.616065	0.001536
Colon Transversum	0.246923	3.616065	0.001536
Duodenum	17.148514	1.979037	3.763289
Fat		0.336227	
Gonads	0.905622	9.487275	0.017632
Heart	0.156351	0.236009	0.039339
Kidney	0.143487		0.000844
Large Intestine	0.246923	3.616065	0.001536
Liver Pericentral	11.417733	1.544044	14.787736
Liver Periportal	11.417733	1.544044	14.787736
Lower Ileum	17.148514	1.979037	3.763289
Lower Jejunum	17.148514	1.979037	3.763289
Lung	0.376486	0.222479	0.398131
Muscle	0.125668	0.295222	0.003081
Pancreas	4.089445	0.135632	2.180243
Plasma			0.000578
Rectum		3.616065	
Skin	1.900147		
Small Intestine	17.148514	1.979037	3.763289
Spleen	0.278059		0.005489
Stomach	9.489418	0.500298	1.146997
Upper Ileum	17.148514	1.979037	3.763289
Upper Jejunum	17.148514	1.979037	3.763289

UGT1A1 Expression

PK-Sim Or...	Unit ▲ / Database ▲ / Array / E-GEOD-2361
Bone	1.176133
Brain	1.172059
Colon Ascendens	4.080897
Colon Descenden...	4.080897
Colon Sigmoid / D...	4.080897
Colon Transversum	4.080897
Duodenum	10.331696
Gonads	0.989109
Heart	1.063481
Kidney	14.965333
Large Intestine	4.080897
Liver Pericentral	9.042830
Liver Periportal	9.042830
Lower Ileum	10.331696
Lower Jejunum	10.331696
Lung	0.959113
Muscle	0.953313
Pancreas	1.356025
Skin	2.688076
Small Intestine	10.331696
Spleen	1.152975
Stomach	2.458162
Upper Ileum	10.331696
Upper Jejunum	10.331696

P-glycoprotein Expression

	Unit ▲	Database ▲	
	Array	EST	RT-PCR
PK-Sim Or... ▲	E-GEOD-2361	UNIGENE	NISHIMURA et al...
Bone	0.493518		0.275848
Brain	1.704790	0.971758	0.865462
Cecum		18.835723	
Colon Ascendens	2.526933	18.835723	1.260749
Colon Descenden...	2.526933	18.835723	1.260749
Colon Sigmoid / D...	2.526933	18.835723	1.260749
Colon Transversum	2.526933	18.835723	1.260749
Duodenum	5.579235	18.835723	3.194530
Gonads	1.081079	0.148909	0.198118
Heart	0.952247	0.536495	0.476810
Kidney	3.695432	0.469112	8.066899
Large Intestine	2.526933	18.835723	1.260749
Liver Pericentral	1.552096	0.992714	2.180243
Liver Periportal	1.552096	0.992714	2.180243
Lower Ileum	5.579235	18.835723	3.194530
Lower Jejunum	5.579235	18.835723	3.194530
Lung	0.806277		0.747918
Muscle	0.361297	0.198557	0.145981
Pancreas	0.568123	1.618908	0.162096
Rectum		18.835723	
Skin	0.601793	0.072767	
Small Intestine	5.579235	18.835723	3.194530
Spleen	1.152975		0.844607
Stomach	0.777439		0.296703
Upper Ileum	5.579235	18.835723	3.194530
Upper Jejunum	5.579235	18.835723	3.194530

OATP1B1 Expression

PK-Sim Or...	Unit: Array / Database: E-GEOD-2361	Unit: EST / Database: UNIGENE	Unit: RT-PCR / Database: NISHIMURA et al...
Bone	0.235396		
Brain	0.190699		0.003384
Colon Ascendens	0.058497		
Colon Descenden...	0.058497		
Colon Sigmoid / D...	0.058497		
Colon Transversum	0.058497		
Duodenum	0.140571		
Gonads	0.300826	2.000418	0.338412
Heart	0.414997		0.019717
Kidney	0.180208		
Large Intestine	0.058497		
Liver Pericentral	7.219297	2.480849	23.887881
Liver Periportal	7.219297	2.480849	23.887881
Lower Ileum	0.140571		
Lower Jejunum	0.140571		
Lung	0.164582		0.000957
Muscle	0.109371		0.015451
Pancreas	0.067932		
Skin	0.077773		
Small Intestine	0.140571		
Spleen	0.082271	0.597071	
Stomach	0.073642		
Upper Ileum	0.140571		
Upper Jejunum	0.140571		

Adult ketoconazole and midazolam PBPK model development and evaluation

PK data for ketoconazole and midazolam model development and evaluation were digitized from the literature using Plot Digitizer Version 2.6.8 (Supplemental Table 5). Ketoconazole undergoes oxidation by CYP3A into its major metabolite (M2) along with five other minor metabolites (M3, M6, M7, M8, and M13) (Fitch *et al.*, 2009). Since parameters were not available to describe CYP3A4 CL of ketoconazole, the K_M and V_{max} were initially obtained

from a study describing voriconazole CYP3A4 CL (Hyland *et al.*, 2003). Ketoconazole also undergoes glucuronide conjugation by UDP-glucurosyltransferase 1A4 (UGT1A4) (Bourcier *et al.*, 2010). Protein binding for ketoconazole is concentration dependent (93% at 50 µg/mL and 91% at 25 µg/mL based on equilibrium dialysis), which may contribute to the non-linear kinetics for ketoconazole (Van Tyle, 1984; Huang *et al.*, 1986). Ketoconazole also binds to blood cells resulting in ~1% free drug in plasma (DrugBank, 2020; Van Tyle, 1984). Therefore, protein binding to albumin was manually optimized based on the administered dose, and CYP3A4 V_{max} and UGT1A4 V_{max} were optimized using parameter optimization (Table 1). The Poulin and Theil method was used to calculate partition coefficients and the charge dependent Schmitt normalized to PK-Sim® method was used to calculate cellular permeability (Poulin and Theil, 2000; Open Systems Pharmacology Suite community, 2018). Population simulations based on 100 virtual subjects (white American population from 18 to 46 years of age) receiving 100, 200, 400, and 800 mg PO ketoconazole were performed and were evaluated by visually comparing the simulated mean and associated 90% prediction interval with the observed data from the literature. The mean simulated and observed area under the concentration versus time curve from 0 to 8 hours (AUC_{0-8}) or area under the concentration versus time curve extrapolated to infinity ($AUC_{0-\infty}$), and the maximal concentration (C_{max}) were also compared, with a 2-fold ratio (0.5 to 2-fold ratio) considered acceptable. CYP3A4 competitive inhibition was included based on the formation of 1'-hydroxymidazolam in human liver microsomes from four human donors (Von Moltke *et al.*, 1996). CYP3A5 non-competitive inhibition was included based 1'-hydroxymidazolam formation in c-DNA expressed CYP3A5 microsomal preparations (Gibbs *et al.*, 1999). P-glycoprotein inhibition was included based on a PBPK model that estimated the *in-*

vivo inhibition constant (K_I) for renal P-glycoprotein to describe the clinical DDI between ketoconazole and fesoterodine in healthy adult subjects (Oishi *et al.*, 2018).

The adult PBPK model for midazolam included key drug properties described in Table 1. Protein binding is approximately 97% to human plasma albumin in adults as well as pediatric patients greater than 1 year of age. Studies in human liver microsomes indicate the midazolam is primarily metabolized by CYP3A4 (U.S. Food and Drug Administraiton (FDA), 2017; Xiao *et al.*, 2019). Lipophilicity and transcellular intestinal permeability were optimized using both the IV and PO data with the Monte Carlo algorithm. Partition coefficients were calculated using the Rodgers and Rowland method and cellular permeability was calculated using the PK-Sim® Standard method (Rodgers and Rowland, 2006; Open Systems Pharmacology Suite community, 2018). Population simulations based on 100 virtual subjects (white American population from 18 to 46 years of age) receiving a 2 mg IV infusion over 30 minutes and 15 mg PO midazolam were performed and visually compared with observed data. The simulated versus observed mean $AUC_{0-\infty}$ and C_{max} were also compared, with a 2-fold range considered acceptable. To validate ketoconazole as a CYP3A inhibitor, we simulated the CYP3A mediated DDI between ketoconazole and midazolam in adults and compared with observed data obtained in the literature from clinical studies (Supplemental Table 6).

Individual level concentration versus time data was not available for pediatric patients receiving ketoconazole, so simulated PK parameters were compared with observed PK parameters in children receiving PO ketoconazole from the literature. Population simulations were performed for 100 virtual subjects (5 months to 14 years) receiving 9 mg/kg PO ketoconazole daily for 2 weeks, and the C_{max} and the daily steady-state AUC steady-state ($AUC_{0-24,ss}$) was compared with data from 26 children with candidiasis whom received an average

(range) daily dosage of PO ketoconazole of 9 (6-13) mg/kg (Pietrogrande *et al.*, 1983; Bardare *et al.*, 1984). Population simulations were also performed for 100 virtual subjects from 2 to 12.5 years of age receiving a single 5 mg/kg suspension, and the C_{max} and $AUC_{0-\infty}$ was compared with 12 children with PO candidiasis and superficial dermatophytoses whom received 5 mg/kg ketoconazole suspension (Ginsburg *et al.*, 1983). The transcellular intestinal permeability for ketoconazole was decreased to $2*10^{-4}$ cm/min (fraction absorbed of 0.80) in order to capture the observed AUC and C_{max} in pediatric patients.

Population simulations for midazolam were performed for 100 virtual subjects with similar ages, doses, and formulations as described in the study population reported in the literature (Supplemental Table 5). The midazolam pediatric PBPK model was evaluated by comparing the CL and V to values reported in pediatric patients from 2 days to 16.2 years receiving IV midazolam (Jacqz-Aigrain *et al.*, 1990; Nahara *et al.*, 2000; Reed *et al.*, 2001). We also compared the $AUC_{0-\infty}$ and C_{max} to values reported in pediatric patients from 0.5 to <16 years receiving a single PO dose (0.25 mg/kg, 0.5 mg/kg, and 1.0 mg/kg) of midazolam (Reed *et al.*, 2001). Acceptance criteria was for the simulated CL, V, $AUC_{0-\infty}$ and C_{max} to be within 0.5-2-fold of the observed PK parameters.

Supplementary Results

Ketoconazole and Midazolam Adult PBPK Model

Ketoconazole population simulations were performed in virtual adults receiving single PO doses (100, 200, 400, and 800 mg) of ketoconazole and visually compared with digitized mean observed data in healthy adults (Supplemental Figure 8). Ketoconazole population simulations were also performed in virtual adults receiving 200 mg PO daily and 400 mg PO daily multiple dosing administration, and resulted in reasonable agreement with the digitized

mean data observed in healthy adults (Supplemental Figure 9). Furthermore, the simulated versus observed AUC_{0-8} and C_{max} in 10 adult patients with fungal disease receiving a single 100 mg dose of ketoconazole was 5.30 versus 5.73 µg*h/mL and 1.70 versus 1.60 µg/mL, respectively (Brass *et al.*, 1982). The simulated versus observed $AUC_{0-\infty}$ reported in healthy volunteers receiving a single dose of 200 mg and 400 mg ketoconazole was 23.84 versus 17.55 µg*h/mL and 47.8 versus 40.9 µg*h/mL, respectively (Daneshmend *et al.*, 1981). The simulated versus observed C_{max} in healthy volunteers receiving a single dose of 200 mg ketoconazole was 5.04 versus 3.60 µg/mL and for a single 400 mg dose of ketoconazole was 10.1 versus 6.5 µg/mL, respectively (Daneshmend *et al.*, 1981). Midazolam population simulations were performed for a single dose of 15 mg PO and a single 2 mg IV (30-minute infusion), and resulted in reasonable agreement with the digitized mean data observed in healthy adults (Supplemental Figure 10). Furthermore, the simulated versus observed mean $AUC_{0-\infty}$ and C_{max} for 15 mg PO midazolam (one hour post meal) was 184 versus 184 ng*hr/mL and 41 versus 48 ng/mL, respectively, based on a study conducted in 18 healthy volunteers (Bornemann *et al.*, 1986). Additionally, the simulated versus observed mean $AUC_{0-\infty}$ and C_{max} for 2 mg IV midazolam was 69.61 versus 84.76 ng*hr/mL and 48.40 versus 45.68 ng/mL, respectively, based on a study in 27 healthy adult volunteers (Pentikis *et al.*, 2007).

Ketoconazole and Midazolam Pediatric PBPK Model

After scaling the adult PO ketoconazole PBPK model to pediatric patients from 0.42 to 14 years of age, the AUC and C_{max} was over-predicted by 2-3-fold. For example, the simulated versus observed mean $AUC_{0-24,ss}$ and C_{max} for the 9 mg/kg PO daily ketoconazole dose in infants and children 5 months to 14 years of age was 69.1 versus 32.7 µg*h/mL and 14.6 versus 4.9 µg/mL, respectively. Likewise, the simulated versus observed $AUC_{0-\infty}$ and C_{max} for the 5 mg/kg

PO single dose in children 2 to 12 years of age was 38.7 versus 15.3 µg*h/mL and 7.9 versus 4.4 µg/mL, respectively. Reducing the transcellular intestinal permeability approximately 10-fold from the adult permeability value resulted in similar AUC and C_{max} values as reported in 26 infants and children (0.42 to 14 years of age) with candidiasis (Pietrogrande *et al.*, 1983; Bardare *et al.*, 1984) and 12 children with PO candidiasis and superficial dermatophytoses (Ginsburg *et al.*, 1983) (Supplemental Table 7).

The adult IV and PO midazolam PBPK model was scaled to pediatric patients ranging from 2 days to 16 years of age. The mean CL and volume of distribution at steady-state (V_{ss}) for the pediatric midazolam PBPK model were within 0.67-1.27-fold to values reported in pediatric patients from 2 days to 16.2 years receiving IV midazolam except for the V_{ss} in children from 12 to <16 years (Jacqz-Aigrain *et al.*, 1990; Nahara *et al.*, 2000; Reed *et al.*, 2001) (Supplemental Table 8). The $AUC_{0-\infty}$ and C_{max} were generally within 0.5-2-fold of values reported in pediatric patients from 0.5 to <16 years receiving a single PO dose of midazolam (Reed *et al.*, 2001) (Supplemental Table 9).

References:

Bardare M, Tortorano AM, Pietrogrande MC, and Viviani MA (1984) Pharmacokinetics of ketoconazole and treatment evaluation in candidal infections. *Arch Dis Child* **59**:1068–1071.

Bornemann LD, Crews T, Chen SS, Twardak S, and Patel IH (1986) Influence of food on midazolam absorption. *J Clin Pharmacol* **26**:55–9.

Burchell B, Coughtrie M, Jackson M, Harding D, Fournel-Gigleux S, Leakey J, and Hume R (1989) Development of human liver UDP glucuronosyltransferases. *Dev Pharmacol Ther*: 70-77.

Chung E, Nafziger AN, Kazierad DJ, and Bertino JS (2006) Comparison of midazolam and simvastatin as cytochrome P450 3A probes. *Clin Pharmacol Ther* **79**:350–361.

Daneshmend TK, Warnock DW, Ene MD, Johnson EM, Parker G, Richardson MD, and Roberts CJC (1983) Multiple dose pharmacokinetics of ketoconazole and their effects on antipyrine kinetics in man. *J Antimicrob Chemother* **12**:185–188.

Daneshmend TK, Warnock DW, Turner A, and Roberts CJC (1981) Pharmacokinetics of ketoconazole in normal subjects. *J Antimicrob Chemother* **8**:299–304.

Ginsburg CM, McCracken GH, and Olsen K (1983) Pharmacology of ketoconazole suspension in infants and children. *Antimicrob Agents Chemother* **23**:787–789.

Gonzalez D, James LP, Al-Uzri A, Bosheva M, Adler-Shohet FC, Mendley SR, Bradley JS, Espinosa C, Tsonkova E, Moffett K, Marquez L, Simonsen KA, Stoilov S, Boakye-Agyeman F, Jasion T, Hornik CP, Hernandez R, Benjamin DK, and Cohen-Wolkowiez M

(2018) Population pharmacokinetics and safety of solithromycin following intravenous and oral administration in infants, children, and adolescents. *Antimicrob Agents Chemother* **62(8):** e00692-18**.**

Huang Y -C, Colaizzi JL, Bierman RH, Woestenborghs R, and Heykants JJP (1986) Pharmacokinetics and dose proportionality of ketoconazole in normal volunteers. *Antimicrob Agents Chemother* **30**:206–210.

Jacqz-Aigrain E, Wood C, and Robieux I (1990) Pharmacokinetics of midazolam in critically ill neonates. *Eur J Clin Pharmacol* **39**:191–2.

Jiang X-L, Zhao P, Barrett JS, Lesko LJ, and Schmidt S (2013) Application of physiologically based pharmacokinetic modeling to predict acetaminophen metabolism and pharmacokinetics in children. *CPT pharmacometrics Syst Pharmacol* **2**:e80.

Johnson TN, Tanner MS, Taylor CJ, and Tucker GT (2001) Enterocytic CYP3A4 in a paediatric population: Developmental changes and the effect of coeliac disease and cystic fibrosis. *Br J Clin Pharmacol* **51**:451–460.

Johnson TN, Zhou D, and Bui KH (2014) Development of physiologically based pharmacokinetic model to evaluate the relative systemic exposure to quetiapine after administration of IR and XR formulations to adults, children and adolescents. *Biopharm Drug Dispos* **35**:341–52.

Juif P-E, Boehler M, Donazzolo Y, Bruderer S, and Dingemanse J (2017) A pharmacokinetic drug–drug interaction study between selexipag and midazolam, a CYP3A4 substrate, in healthy male subjects. *Eur J Clin Pharmacol* **73**:1121–1128.

Lacroix D, Sonnier M, Moncion A, Cheron G, and Cresteil T (1997) Expression of CYP3A in the human liver - Evidence that the shift between CYP3A7 and CYP3A4 occurs immediately after birth. *Eur J Biochem* **247**:625–634.

Lam YWF, Alfaro CL, Ereshefsky L, and Miller M (2003) Pharmacokinetic and pharmacodynamic interactions of oral midazolam with ketoconazole, fluoxetine, fluvoxamine, and nefazodone. *J Clin Pharmacol* **43**:1274–1282.

Ma JD, Nafziger AN, Rhodes G, Liu S, and Bertino JS (2006) Duration of pleconaril effect on cytochrome P450 3A activity in healthy adults using the oral biomarker midazolam. *Drug Metab Dispos* **34**:783–785.

Mannisto PT, Mantyla R, Nykanen S, Lamminsivu U, and Ottoila P (1982) Impairing effect of food on ketoconazole absorption. *Antimicrob Agents Chemother* **21**:730–733.

Meyer M, Schneckener S, Ludewig B, Kuepfer L, and Lippert J (2012) Using expression data for quantification of active processes in physiologically based pharmacokinetic modeling. *Drug Metab Dispos* **40**:892–901.

Misaka S, Uchida S, Imai H, Inui N, Nishio S, Ohashi K, Watanabe H, and Yamada S (2010) Pharmacokinetics and pharmacodynamics of low doses of midazolam administered intravenously and orally to healthy volunteers. *Clin Exp Pharmacol Physiol* **37**:290–295.

Nahara MC, McMorrow J, Jones PR, Anglin D, and Rosenberg R (2000) Pharmacokinetics of midazolam in critically ill pediatric patients. *Eur J Drug Metab Pharmacokinet* **25**:219–221.

Oldach D, Clark K, Schranz J, Das A, Craft JC, Scott D, Jamieson BD, and Fernandes P (2013) Randomized, double-blind, multicenter phase 2 study comparing the efficacy and safety of

oral solithromycin (CEM-101) to those of oral levofloxacin in the treatment of patients with community-acquired bacterial pneumonia. *Antimicrob Agents Chemother* **57**:2526–34\.

Olkkola KT, Backman JT, and Neuvonen PJ (1994) Midazolarn should be avoided in patients receiving the systemic antimycotics ketoconazole or itraconazole. *Clin Pharmacol Ther* **55**:481–485.

Onishi S, Kawade N, Itoh S, Isobe K, and Sugiyama S (1979) Postnatal development of uridine diphosphate glucuronyltransferase activity towards bilirubin and 2 aminophenol in human liver. *Biochem J* **184**:705–707,.

Pentikis HS, Connolly M, Trapnell CB, Forbes WP, and Bettenhausen DK (2007) The effect of multiple-dose, oral rifaximin on the pharmacokinetics of intravenous and oral midazolam in healthy volunteers. *Pharmacotherapy* **27**:1361–1369.

Pietrogrande MC, Tortorano AM, Viviani MA, Cohen E, and Bardare M (1983) Ketoconazole treatment of candidiasis in children: clinico-pharmacokinetic study. *Pediatr Med Chir* **5**:91–4.

PK-Sim (2017). PK-Sim ® Ontogeny Database. **Version 7.**:1–47.

Reed MD, Rodarte A, Blumer JL, Khoo KC, Akbari B, Pou S, and Kearns GL (2001) The single-dose pharmacokinetics of midazolam and its primary metabolite in pediatric patients after oral and intravenous administration. *J Clin Pharmacol* **41**:1359–1369.

Rodvold KA, Gotfried MH, Still JG, Clark K, and Fernandes P (2012) Comparison of plasma, epithelial lining fluid, and alveolar macrophage concentrations of solithromycin (CEM-101) in healthy adult subjects. *Antimicrob Agents Chemother* **56**:5076–81.

Salem F, Johnson TN, Abduljalil K, Tucker GT, and Rostami-Hodjegan A (2014) A re-evaluation and validation of ontogeny functions for cytochrome P450 1A2 and 3A4 based on in vivo data. *Clin Pharmacokinet* **53**:625–36.

Salerno SN, Edginton A, Cohen-Wolkowiez M, Hornik CP, Watt KM, Jamieson BD, and Gonzalez D (2017) Development of an Adult Physiologically Based Pharmacokinetic Model of Solithromycin in Plasma and Epithelial Lining Fluid. *CPT Pharmacometrics Syst Pharmacol* **6(12)**: 814-822.

Stevens JC, Hines RN, Gu C, Koukouritaki SB, Manro JR, Tandler PJ, and Zaya MJ (2003) Developmental expression of the major human hepatic CYP3A enzymes. *J Pharmacol Exp Ther* **307**:573–582.

Still JG, Schranz J, Degenhardt TP, Scott D, Fernandes P, Gutierrez MJ, and Clark K (2011) Pharmacokinetics of solithromycin (CEM-101) after single or multiple oral doses and effects of food on single-dose bioavailability in healthy adult subjects. *Antimicrob Agents Chemother* **55**:1997–2003.

Thelen K, Coboeken K, Willmann S, Burghaus R, Dressman JB, and Lippert J (2011) Evolution of a detailed physiological model to simulate the gastrointestinal transit and absorption process in humans, Part 1: Oral solutions. *J Pharm Sci* **100**:5324–5345.

Tiseo PJ, Perdomo CA, and Friedhoff LT (1998) Concurrent administration of donepezil HCl and ketoconazole: Assessment of pharmacokinetic changes following single and multiple doses. *Br J Clin Pharmacol* **46**:30–34.

Tréluyer JM, Bowers G, Cazali N, Sonnier M, Rey E, Pons G, and Cresteil T (2003) Oxidative metabolism of amprenavir in the human liver. Effect of the CYP3A maturation. *Drug*

Metab Dispos **31**:275–281.

Tsunoda SM, Velez RL, von Moltke LL, and Greenblatt DJ (1999) Differentiation of intestinal and hepatic cytochrome P450 3A activity with use of midazolam as an in vivo probe: Effect of ketoconazole. *Clin Pharmacol Ther* **66**:461–471.

Upreti V V, and Wahlstrom JL (2016) Meta-analysis of hepatic cytochrome P450 ontogeny to underwrite the prediction of pediatric pharmacokinetics using physiologically based pharmacokinetic modeling. *J Clin Pharmacol* **56**:266–83.

Van Tyle JH Van (1984) Ketoconazole mechanism of action, spectrum of activity, drug interactions, adverse reactions and therapeutic use. *Pharmacotherapy* **4**:343–373.

Veldhorst-Janssen NML, Fiddelers AAA, van der Kuy P-HM, Theunissen HMS, de Krom MCTFM, Neef C, and Marcus MAE (2011) Pharmacokinetics and Tolerability of Nasal Versus Intravenous Midazolam in Healthy Dutch Volunteers: A Single-Dose, Randomized-Sequence, Open-Label, 2-Period Crossover Pilot Study. *Clin Ther* **33**:2022–2028.

Winter H, Egizi E, Erondu N, Ginsberg A, Rouse DJ, Severynse-Stevens D, Pauli E, and Everitt D (2013) Evaluation of Pharmacokinetic Interaction between PA-824 and Midazolam in Healthy Adult Subjects. *Antimicrob Agents Chemother* **57**:3699–3703.

Zhou W, Johnson TN, Xu H, Cheung S, Bui KH, Li J, Al-Huniti N, and Zhou D (2016) Predictive Performance of Physiologically Based Pharmacokinetic and Population Pharmacokinetic Modeling of Renally Cleared Drugs in Children. *CPT pharmacometrics Syst Pharmacol* **5**:475–83.

Supplementary Tables and Figures

Supplemental Table 1. Clinical data used for physiologically-based pharmacokinetic (PBPK) model development.

Study	**CE01-102** (Still *et al.*, 2011)	**CE01-121** **(**Sponsor data on file)	**CE01-110** (Sponsor data on file)	**CE01-114** (Rodvold *et al.*, 2012)	**CE01-200** (Oldach *et al.*, 2013)
Trial phase	1	1	1	1	2
Number of Adult Subjects	25	30	14	31	65[2]
Regimen	200, 400, and 600 mg daily for 7 days	400 mg daily x 7 days; 800mg single-dose	800 mg on day 1, 400 mg daily x 4 days	400 mg daily x 5 days	800 mg on day 1, 400 mg daily x 4 days
Formulation[a]	PO	IV	PO	PO	PO
% Female	27%	23%	54%	19%	57%
Age (years)	32.9 (20-55)	44.6 (23-59)	34.2 (21-43)	33.6 (19-46)	56.0 (25-87)
Weight (kg)	74.5 (61.4-90.3)	82.75 (66-102)	76.2 (61.5-95.6)	82.2 (58.1-97)	N/A
Plasma Samples	676	801	356	31	102

[a]Formulation: capsule (PO) or Intravenous suspension (IV). [2]Pharmacokinetic (PK) data was available for 22 of these subjects. Data presented as the average (range).

Supplemental Table 2. Comparison of adult clearance values for solithromycin between the observed data and the simulated PBPK model.

	CL/F or CL on Day 1 (L/h)						CL/F or CL after multiple doses (L/h)					
	Observed data		PBPK model				Observed data		PBPK model			
Dosing Regimen	**Mean**	**SD**	**Mean**	**SD**	**Ratio**	**SD**	**Mean**	**SD**	**Mean**	**SD**	**Ratio**	**SD**
200 mg PO daily	267	140	132	22	0.5	0.3	102	60	116	26	1.1	0.7
400 mg PO daily	103	141	125	22	1.2	1.7	96	198	77	48	0.8	1.7
600 mg PO daily	131	178	119	24	0.9	1.2	35	11	26	31	0.7	0.9
800 mg PO day 1, 400 mg PO day 2-5	61	54	111	33	1.8	1.7	32	13	75	34	2.3	1.8
400 mg IV daily	70	17	70	10	1.0	0.3	34	13	50	26	1.5	0.9
800 mg IV day 1	42	8	66	14	1.6	0.4	N/A	N/A	N/A	N/A	N/A	N/A

The ratio was calculated as the ratio of mean predicted values over mean observed values with a ratio for the standard deviation as described previously (Jiang *et al.*, 2013; Johnson *et al.*, 2014; Zhou *et al.*, 2016). There were 45%, 64%, and 91% of simulated CL or CL/F values within 1.33, 1.5, and 2.0-fold of the observed CL or CL/F values. Abbreviations: CL/F: clearance following oral administration; CL: clearance; PBPK: physiologically-based pharmacokinetic model; SD: standard deviation; PO: oral

Supplemental Table 3. Average fold errors for the solithromycin physiologically-based pharmacokinetic (PBPK) model.

Population	Dosing and Administration	Average Fold Error
Healthy Adults	200 mg PO daily	1.43
Healthy Adults	400 mg PO daily	1.00
Healthy Adults	600 mg PO daily	2.23
Healthy Adults	800 mg PO day 1, 400 mg PO day 2-5	0.78
Healthy Adults	400 mg IV daily	0.97
Healthy Adults	800 mg IV day 1	0.63
Pediatric Patients	IV Formulation	0.61
Pediatric Patients	Oral Suspension	0.83
Pediatric Patients	Oral Capsules	0.56

The adult model was evaluated using plasma concentration data from 100 healthy subjects and 22 patients with community acquired bacterial pneumonia (CABP) (1,966 plasma samples) as described previously (Supplemental Table 1) (Salerno *et al.*, 2017). The solithromycin pediatric PBPK model was evaluated using 684 plasma concentration data available from 96 pediatric patients ranging from 4 days to 17.9 years. The pediatric concentration data was normalized to a 1 mg/kg dose. The average fold error was calculated for each dosing regimen according to the equation where predicted is the simulated geometric mean value for adults and the arithmetic mean value for pediatric subjects: $10^{\left(\frac{1}{n}\right)*\Sigma \log\left(\frac{\text{predicted}}{\text{observed}}\right)}$. Overall, 89%, 56%, and 44% of the average fold error values comparing observed and simulated concentrations across all adult and pediatric dosing regimens were within 2.0-fold, 1.5-fold, and 1.33-fold, respectively.

Supplemental Table 4. Comparison of the population pharmacokinetic (PopPK) and physiologically-based pharmacokinetic (PBPK) model weight-normalized clearance estimates.

Cohort	PopPK estimates[1] CL (L/h/kg)	PBPK Simulated CL day 1 (L/h/kg)	PBPK Simulated CL day 5 (L/h/kg)
12 to 17 years (IV)	0.78 (0.19-2.00)	0.88 (0.20-1.63)	0.62 (0.08-1.55)
6 to <12 years (IV)	1.20 (0.43-2.50)	1.14 (0.14, 2.07)	0.85 (0.07, 1.93)
2 to <6 years (IV)	0.53 (0.18-2.40)	1.37 (0.43-2.26)	0.96 (0.08-2.11)
0 to <2 years (IV)	0.87 (0.28-1.40)	1-6 months: 1.05 (0.07-1.90) 0.5-2 years: 1.25 (0.19-2.06)	1-6 months: 0.46 (0.06-1.83) 0.5-2 years: 0.96 (0.08-1.85)

Clearance values are reported as the median (range).

[1]Individual empirical Bayesian post-hoc parameter estimates were obtained based on a published population pharmacokinetic (PopPK) model developed using plasma data from these 96 children (780 plasma samples). The structural model was a 2-compartment model with linear elimination and first-order absorption with an oral absorption lag time. Significant covariates included body weight and a sigmoidal maturation function for post-menstrual age on clearance and weight on the volume of distribution. Modeling time-dependent inhibition did not improve the model fits in these pediatric patients so only one individual clearance value was reported per subject (Gonzalez *et al.*, 2018). Abbreviations: IV: intravenous; CL: clearance.

Supplemental Table 5. Clinical data for ketoconazole and midazolam physiologically-based pharmacokinetic (PBPK) model development and evaluation.

N, Population[a]	Study Drug	Dose and Administration	Reference
23 healthy males 20 (18-25) years	Ketoconazole	200 mg PO tablet, suspension, and solution, fasted; 400 mg PO solution, 800 mg PO solution; single dose	(Huang *et al.*, 1986)
6 healthy males 28-44 years	Ketoconazole	200 mg and 400 mg PO tablet, single, administered with standard breakfast	(Daneshmend *et al.*, 1981)
Healthy adults	Ketoconazole	100 mg, 200 mg, 400 mg tablet, 200 mg solution, single dose	(Van Tyle, 1984)
8 Healthy males 25 (21-46) years	Ketoconazole	200 mg tablets PO twice daily for 5 days, fasted on day 1, breakfast allowed on day 5	(Daneshmend *et al.*, 1983)
10 healthy adults 24 (22-26) years	Ketoconazole	200 mg tablet, fasting, orange juice, standard breakfast, single dose	(Mannisto *et al.*, 1982)
21 healthy adults 31.2 (20-45) years	Ketoconazole	200 mg PO tablets daily for 7 days, fasted	(Tiseo *et al.*, 1998)
26 children with candidiasis (0.42-14 years)	Ketoconazole	daily doses ranged from 3-13 mg/kg (suspension or tablet) for 7 days to 18 months	(Pietrogrande *et al.*, 1983; Bardare *et al.*, 1984)
12 children 6 (2-12.5) years	Ketoconazole	5 mg/kg crushed tablets or suspension, fasted, single dose	(Ginsburg *et al.*, 1983)
27 healthy adults 27.6 (18-51) years	Midazolam	2 mg IV over 30 minutes, single 6 mg PO, single dose	(Pentikis *et al.*, 2007)
9 healthy adults 34.1 (25-55) years	Midazolam	2.5 mg IV bolus, single dose	(Veldhorst-Janssen *et al.*, 2011)
5 males 22.4 ± 6.4 years[b]	Midazolam	5, 15 and 30 µg/kg IV bolus, single 15, 50 and 100 µg/kg PO, single dose	(Misaka *et al.*, 2010)
18 healthy adults 32 (19-46) years	Midazolam	15 mg PO, single dose	(Bornemann *et al.*, 1986)
18 healthy males 27 (20-44) years[c]	Midazolam	7.5 mg PO, single dose	(Juif *et al.*, 2017)
14 healthy adults 27.2 (19-46) years	Midazolam	2 mg PO syrup, single dose	(Winter *et al.*, 2013)
18 healthy adults 31 (21-49) years[c]	Midazolam	0.075 mg/kg PO, single dose	(Ma *et al.*, 2006)

9 healthy adults 26 (19-41) years	Midazolam	2 mg IV, single dose 6 mg PO, single dose	(Tsunoda *et al.*, 1999)
87 children from 6 months to < 16 years of age	Midazolam	0.25, 0.5, or 1 mg/kg (40 mg maximum) oral syrup and 0.15 mg/kg single IV bolus dose	(Reed *et al.*, 2001)
10 critically ill neonates 2-10 post-natal days and 37 34-41 weeks gestational age	Midazolam	0.2 mg/kg single IV bolus dose	(Jacqz-Aigrain *et al.*, 1990)
23 critically ill children 3.6 years (8 days-16.2 years)	Midazolam	49-385 µg/kg/hr IV continuous infusion for 0.3-10.9 hours	(Nahara *et al.*, 2000)

[a]Age presented as mean (range), mean ± standard deviation[b], or median (range)[c] as presented in the original publication.

Abbreviations: N: number of subjects; IV: intravenous; PO: oral

Supplemental Table 6. Adult drug-drug interaction (DDI) predictions for midazolam plus ketoconazole.

	Observed Values		Simulated Values		
Dosing Regimen	**$AUC_{0-\infty}$ Fold**	**C_{max} Fold**	**$AUC_{0-\infty}$ Fold**	**C_{max} Fold**	**Reference**
midazolam 7.5 mg PO ± 400 mg PO daily ketoconazole x 4 days[a]	15.9	4.1	7.8	3.8	(Olkkola *et al.*, 1994)
2 mg IV midazolam bolus ± 200 mg ketoconazole x 3 days[b]	5.0	N/A	3.2	N/A	(Tsunoda *et al.*, 1999)
6 mg PO midazolam ± 200 mg ketoconazole x 3 days[b]	13.6	4.2	8.6	4.0	(Tsunoda *et al.*, 1999)
10 mg PO midazolam ± 200 mg PO ketoconazole daily x 12 days[c]	6.6	3.0	5.6	3.4	(Lam *et al.*, 2003)
0.075 mg/kg midazolam ± 400 mg ketoconazole x 10 days[d]	9.5	2.4	9.1	4.0	(Chung *et al.*, 2006)

[a]Nine healthy adult volunteers received oral ketoconazole (400 mg daily) or placebo for 4 days, and then a single dose of 7.5 mg oral midazolam was administered on day 4 (Olkkola *et al.*, 1994).

[b]Nine healthy individuals received single doses of 2 mg intravenous or 6 mg oral midazolam alone and then single doses of 2 mg intravenous or 6 mg oral midazolam after 3 daily doses of 200 mg oral ketoconazole (Tsunoda *et al.*, 1999**).**

[c]Forty healthy subjects received single 10 mg oral midazolam solutions before and after 12 daily doses of 200 mg ketoconazole (Lam *et al.*, 2003**).**

[d]Nineteen subjects received single oral doses of 0.075 mg/kg midazolam before and after 10 daily doses of 400 mg oral ketoconazole (Chung *et al.*, 2006**).**

Data is presented as the mean fold change for midazolam plus ketoconazole relative to midazolam alone based on simulations using a mean individual (32 year-old white American male, weight of 81 kg, height of 178 cm, body mass index of 25.48 kg/m^2). Abbreviations: $AUC_{0-\infty:}$ area under the curve from zero to infinity; C_{max}: maximal concentration; PO: oral; IV: intravenous.

Supplemental Table 7. Ketoconazole pediatric physiologically-based pharmacokinetic (PBPK) model evaluation.

Dosing Regimen	**Age Range**	**AUC (µg*h/mL)**		**C_{max} (µg/mL)**	
		Simulated	Observed	Simulated	Observed
9 mg/kg PO daily, tablets or suspension (Pietrogrande *et al.*, 1983; Bardare *et al.*, 1984)	0.42 - 14 years	33.5 (5.9-85.3)	32.7 (5.9-82.0)	5.7 (0.93-14.1)	4.9 (1.2-14.0)
5 mg/kg PO single, suspension (Ginsburg *et al.*, 1983)	2 - 12.5 years	23.6 (4.1-70.3)	15.3 (2.6-36.4)	4.1 (0.8-9.3)	4.4 (0.3-8.8)

Data presented as the mean (range). AUC: area under the concentration versus time curve from 0 to 24 hours at steady-state for multiple dosing or 0 to infinity for single dose administration, C_{max}, maximal concentration. Abbreviations: GA: gestational age; PNA: post-natal age.

Supplemental Table 8. Midazolam pediatric pharmacokinetic (PK) parameters for children receiving intravenous midazolam.

Reference	Age Range	CL (L/h/kg)		V (L/kg)	
		Simulated	Observed	Simulated	Observed
(Jacqz-Aigrain *et al.*, 1990)	2-5 days PNA 37 (34-41) weeks GA	0.08 ± 0.02	0.12 ± 0.07	0.7 ± 0.1	0.9 ± 0.4
(Reed *et al.*, 2001)	0.5 to < 2 years	0.57 ± 0.20	0.68 ± 0.38	2.8 ± 1.0	2.2 ± 0.5
(Reed *et al.*, 2001)	2 to < 12 years	0.65 ± 0.20	0.60 ± 0.23	2.6 ± 1.1	2.5 ± 1.4
(Reed *et al.*, 2001)	12 to < 16 years	0.48 ± 0.14	0.56 ± 0.23	1.3 ± 0.4	3.6 ± 1.5
(Nahara *et al.*, 2000)	8 days – 16.2 years	0.08 to 1.12	0.1 to 3.1	0.6 to 5.1	0.2 to 3.5

Data is presented as the mean (±standard deviation) for all studies except for (Nahara *et al.*, 2000), where the data was presented as the range. Abbreviations: CL: clearance; V: volume of distribution; L: liters; h: hour; kg: kilogram; PNA: post-natal age; GA: gestational age.

Supplemental Table 9. Midazolam pediatric physiologically-based pharmacokinetic (PBPK) model predictions for children receiving oral midazolam.

Dosing Regimen and Reference	**Age Range**	**$AUC_{0-\infty}$ (ng*h/mL)**		**C_{max} (ng/mL)**	
		Simulated	Observed	Simulated	Observed
0.25 mg/kg PO single (Reed *et al.*, 2001)	0.5 to < 16 years	278 ± 160	137 ± 86	64 ± 41	56 ± 30
0.5 mg/kg PO single (Reed *et al.*, 2001)	0.5 to < 16 years	388 ± 275	356 ± 320	77 ± 54	123 ± 76
1.0 mg/kg PO single (Reed *et al.*, 2001)	0.5 to < 16 years	563 ± 375	684 ± 581	87 ± 63	186 ± 99

Data is presented as the mean ± standard deviation. Abbreviations: $AUC_{0-\infty}$: area under the concentration versus time curve from 0 to infinity; C_{max}: maximal concentration: PO: oral.

Supplemental Figure 1. Cytochrome P450 3A4 (CYP3A4) time-dependent inhibition.

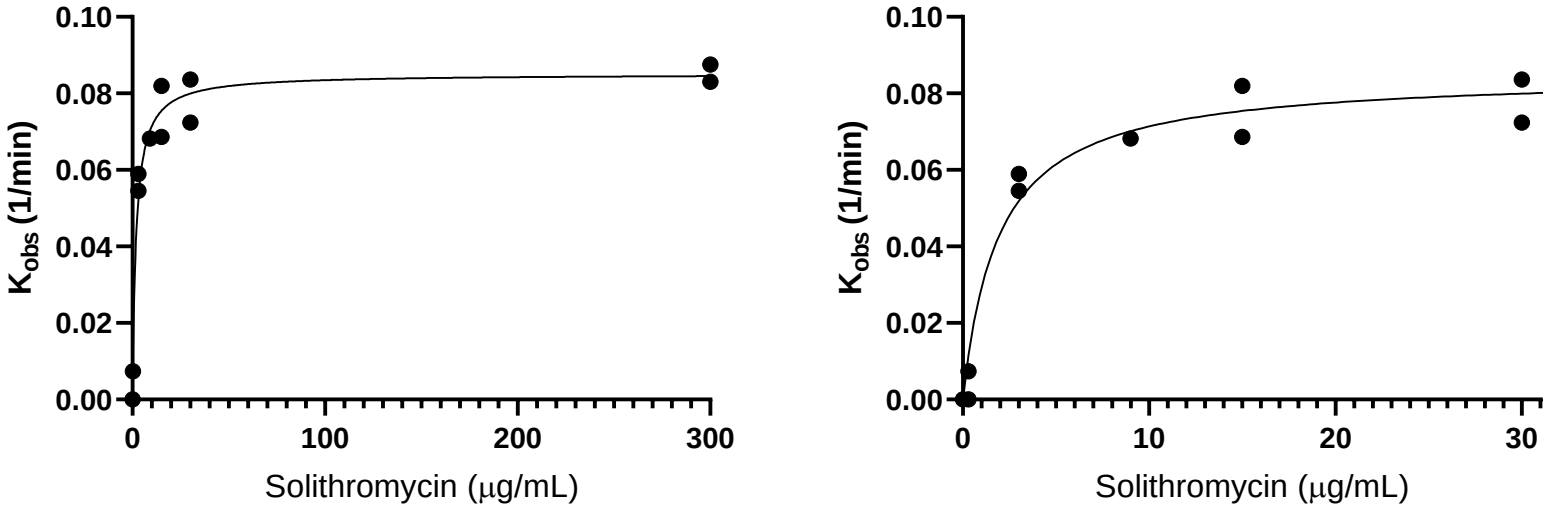

CYP3A4 (200 pmol/mL) was pre-incubated at 37 degrees Celsius with solithromycin (0, 0.3, 3, 9, 15, 30, and 300 µg/mL) for 0, 2.5, 5, 10, 15, and 30 minutes, and then diluted 10-fold into fresh buffer containing 250 µM testosterone and incubated at 37 degrees Celsius for five minutes. Remaining enzymatic activity was measured by the formation of 6β-hydroxy-testosterone using a validated high-performance liquid chromatography-tandem mass spectrometry (HPLC/MS/MS) assay. Each data point represents the mean of duplicates and data from two independent experiments are shown. The negative slope of the natural log of the percent activity remaining at each pre-incubation time, the pseudo first-order rate constant of inactivation (K_{obs}), was plotted against solithromycin concentration.

Supplemental Figure 2. Cytochrome P450 3A5 (CYP3A5) time-dependent inhibition.

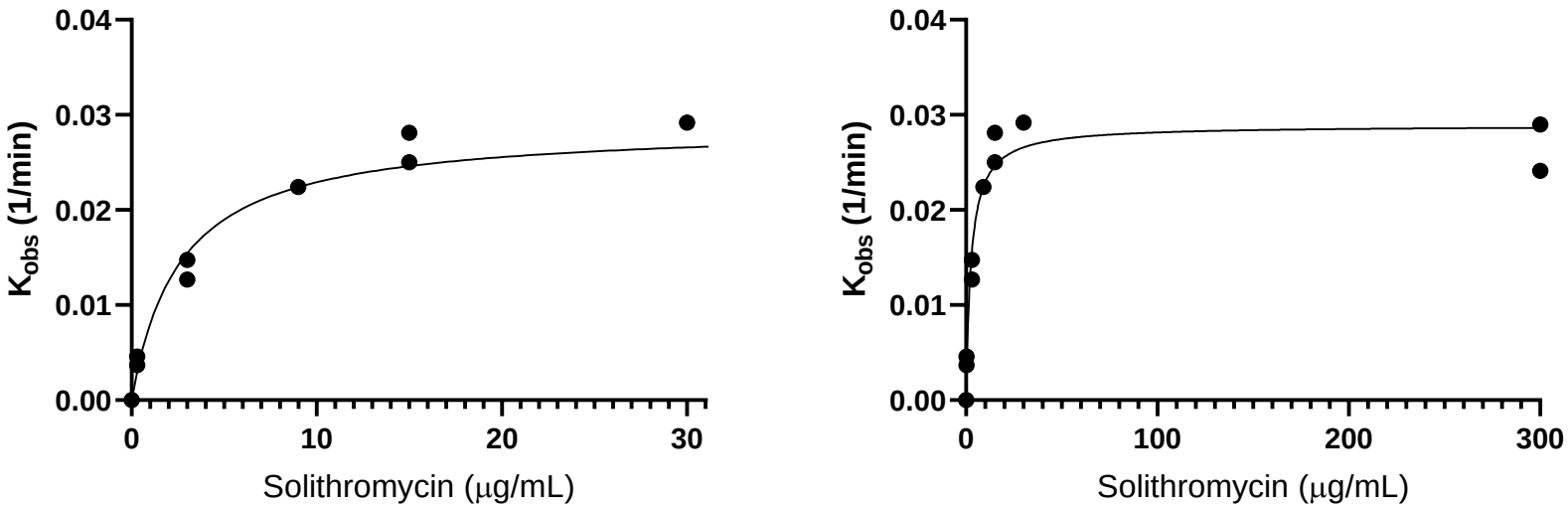

CYP3A5 (200 pmol/mL) was pre-incubated at 37 degrees Celsius with solithromycin (0, 0.3, 3, 9, 15, 30, and 300 μg/mL) for 0, 2.5, 5, 10, 15, and 30 minutes, and then diluted 10 fold into fresh buffer containing 250 μM testosterone and incubated at 37 degrees Celsius for five minutes. Remaining enzymatic activity was measured by the formation of 6β-hydroxy-testosterone using a validated high-performance liquid chromatography-tandem mass spectrometry (HPLC/MS/MS) assay. Each data point represents the mean of duplicates and data from two independent experiments are shown. The negative slope of the natural log of the percent activity remaining at each pre-incubation time, the pseudo first-order rate constant of inactivation (K_{obs}), was plotted against solithromycin concentration.

Supplemental Figure 3. Cytochrome P450 3A7 (CYP3A7) time-dependent inhibition.

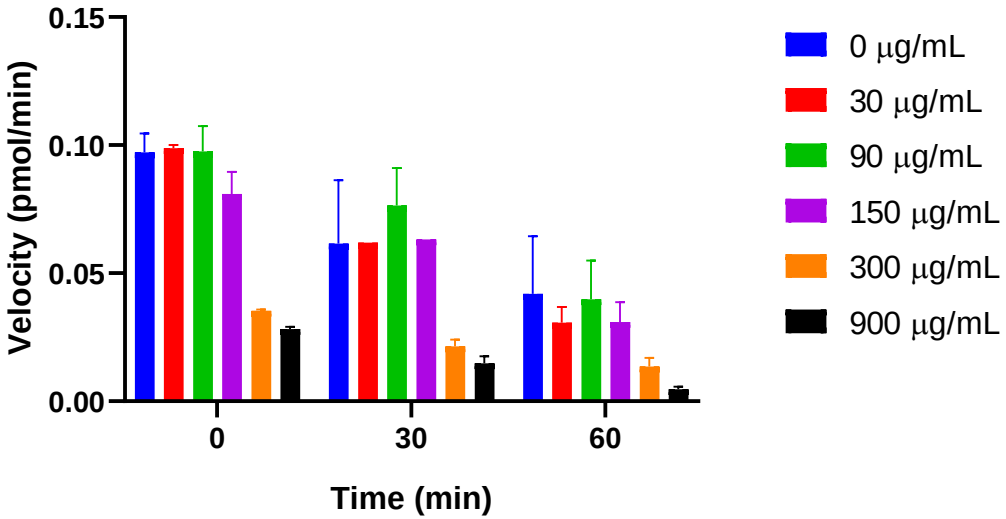

CYP3A7 (400 pmol/mL) was pre-incubated at 37 degrees Celsius with solithromycin (0, 30, 90, 150, 300, and 900 µg/mL). After 0, 5, 15, 30, 45, and 60 minutes, the pre-incubations were diluted 10 fold into fresh buffer containing 250 µM testosterone and incubated at 37 degrees Celsius for 30 minutes. Remaining enzymatic activity was measured by the formation of 6β-hydroxy-testosterone using a validated high-performance liquid chromatography-tandem mass spectrometry (HPLC/MS/MS) assay. Velocity for formation of 6β-hydroxy-testosterone versus time are shown with the mean and standard error of triplicates from a single experiment.

Supplemental Figure 4. CYP3A4/5/7 time linearity for solithromycin metabolite formation.

A)

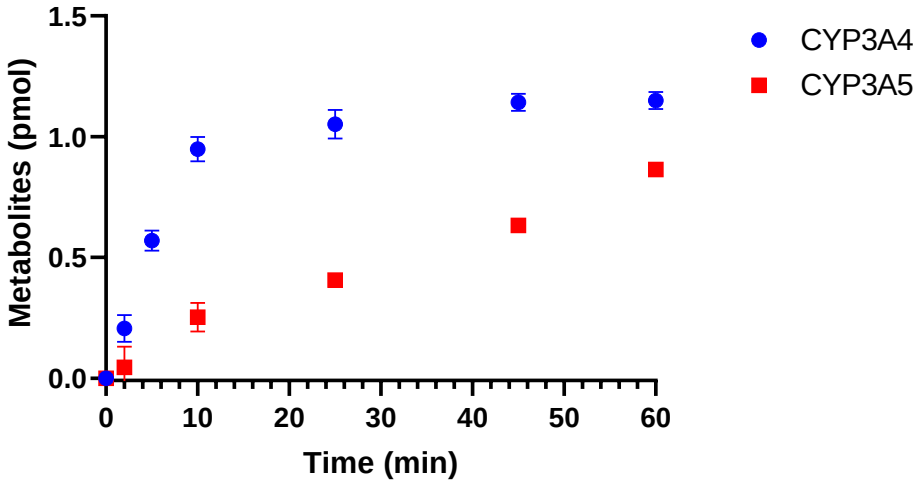

B)

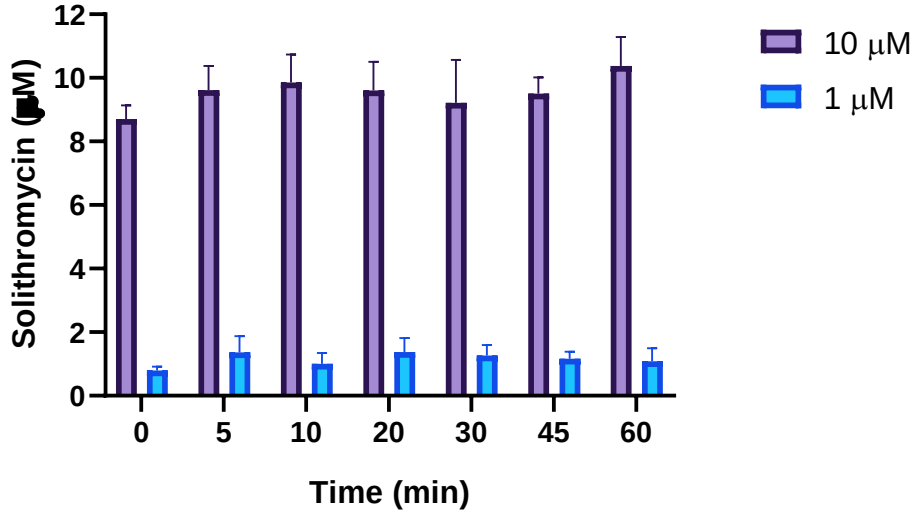

C)

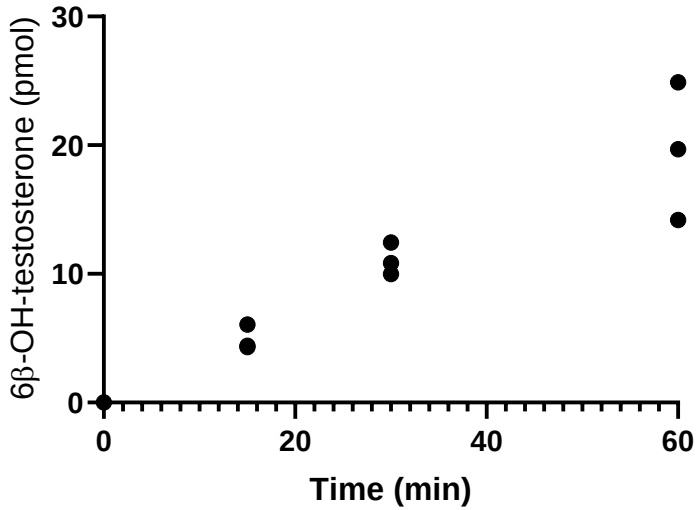

Pilot experiments were first performed to determine the linear range of disappearance of solithromycin. (A) 60 pmol/mL of cytochrome P450 (CYP) 3A4 and CYP3A5 were incubated with 1 µM solithromycin in 100 mM potassium phosphate pH 7.4 plus NADPH Regenerating System Solutions A and B at a dilution of 1:20 and 1:100, respectively, for 0, 2, 5, 10, 15, 30, and 60 minutes. Data is presented as the mean and standard deviation from a single experiment. (B) For CYP3A7, 100 pmol/mL were incubated with 1 µM and 10 µM solithromycin for 0, 5, 10, 15, 20, 30, and 60 minutes. Data is presented as the mean and standard deviation from a single experiment. (C) CYP3A7 was also incubated with 250 µM testosterone for 0, 15, 30, and 60 minutes as a positive control. Data is presented as triplicate samples. The reactions were stopped by a 1:5 dilution into ice-cold methanol containing 0.5 µM

roxithromycin (or 1:4 dilution into acetonitrile containing 0.5 µM 4-androsten-19-1al 3,17-dione), centrifuged at 3500 rpm for 10 minutes at 4 degrees Celsius, and solithromycin and 6β-OH-testosterone were measured in the supernatant by high-performance liquid chromatography-tandem mass spectrometry (HPLC/MS/MS).

Supplemental Figure 5. Cytochrome P450 3A4 (CYP3A4) rate of metabolism (velocity) as a function of solithromycin concentration.

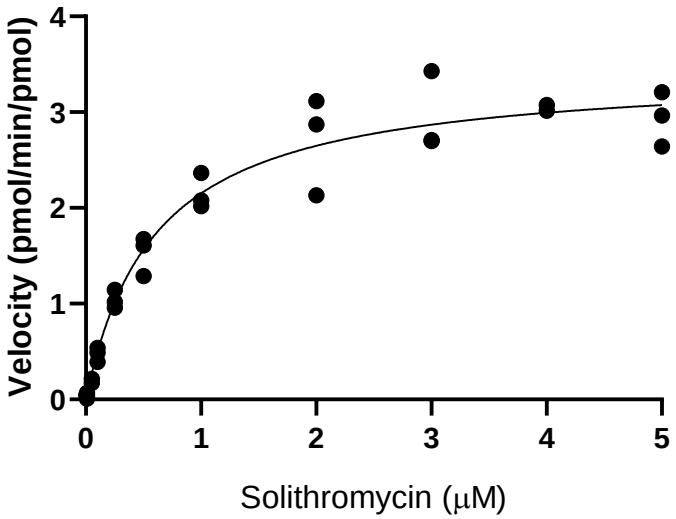

CYP3A4 (60 pmol/mL) was incubated with solithromycin (0.005, 0.01, 0.05, 0.1, 0.25, 0.5, 1, 2, 3, 4, 5 μM) for 2 minutes in order to determine the concentration at half-maximal velocity (K_M)/maximal velocity (V_{max}). Data is presented as the mean of triplicates from three individual experiments.

Supplemental Figure 6. Cytochrome P450 3A5 (CYP3A5) rate of metabolism (velocity) as a function of solithromycin concentration.

A)

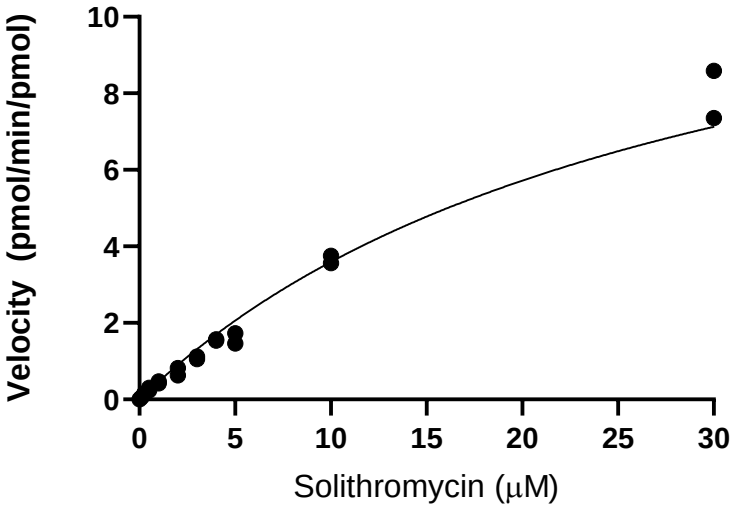

B)

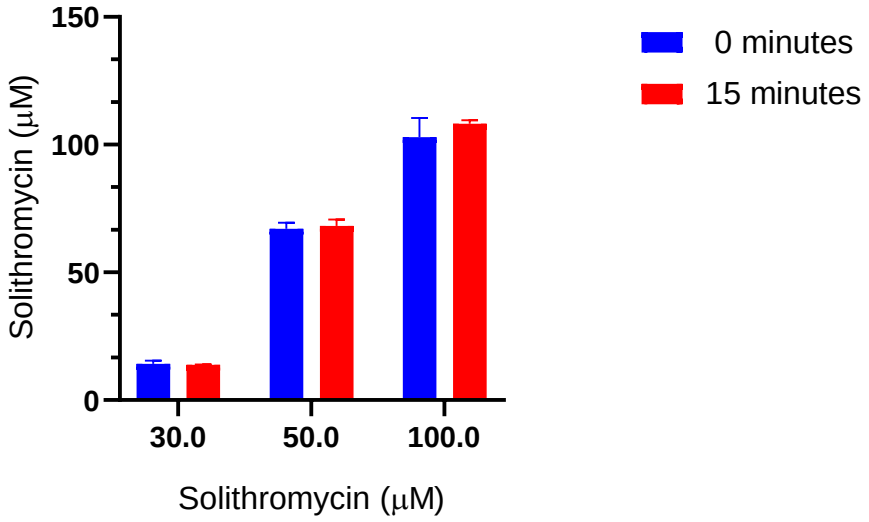

(A) CYP3A5 (60 pmol/mL) was incubated with solithromycin (0.01, 0.05, 0.1, 0.25, 0.5, 1, 2, 3, 4, 5, 10, 30 μM) at 37 degrees Celsius for 15 minutes. Data is presented as the mean of triplicates from two individual experiments. (B) The third experiment for CYP3A5 was conducted at higher concentrations (50 to 3700 μM) to further characterize the maximal velocity (V_{max}), however,

activity starts to decrease >30 μM due to time-dependent inhibition so values beyond 30 μM were not included in determination of concentration at half-maximal velocity $(K_M)/V_{max}$.

Supplemental Figure 7. Population simulations for oral solithromycin in healthy adults.

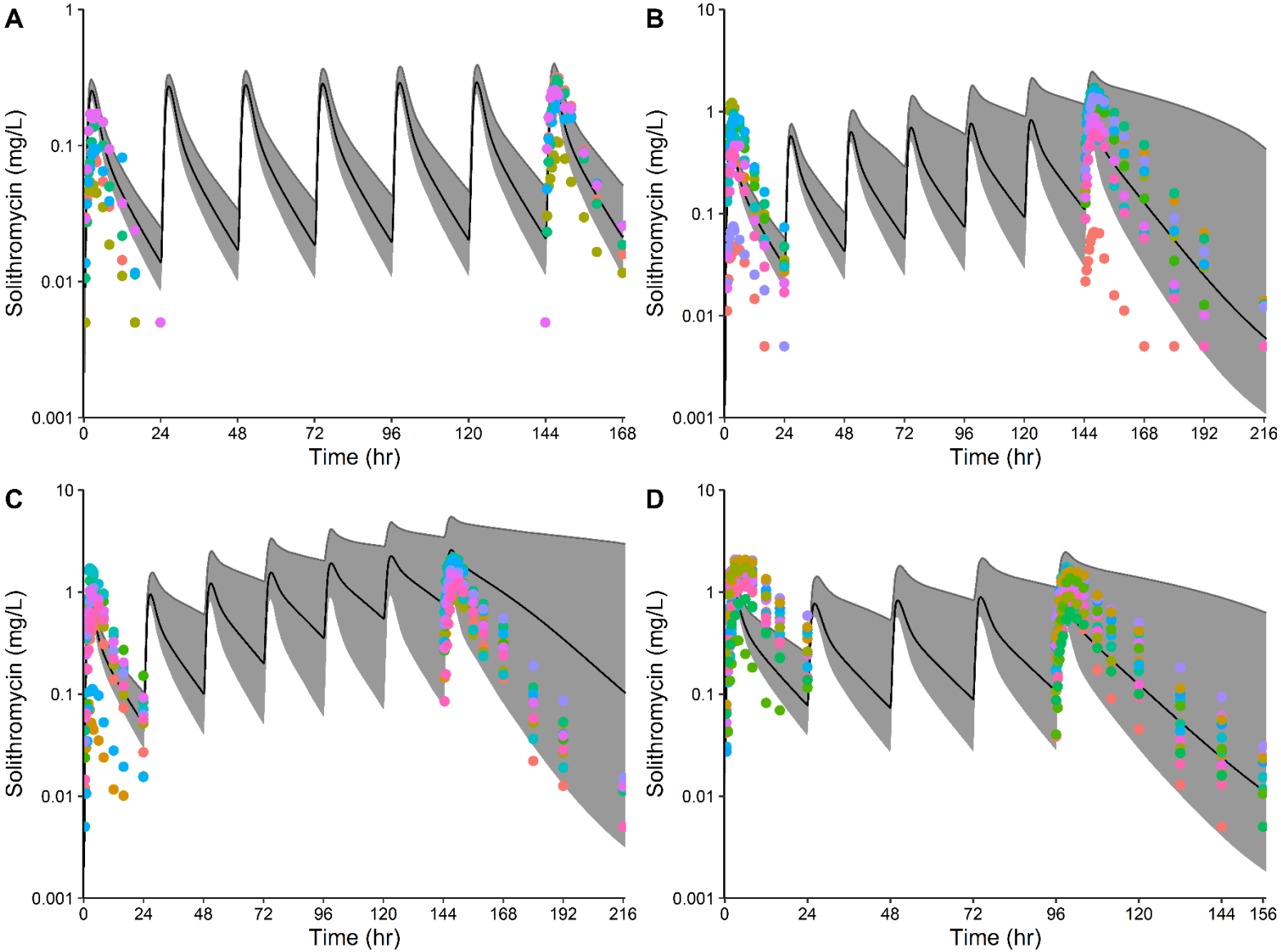

Population simulations were performed for 100 virtual subjects using a Black American population with demographics from study CE01-102 for healthy subjects: 27% female with a mean (range) age of 32.9 (20-55) years and a weight of 74.5 (61.4-90.3) kg. A: 200 mg oral (PO) daily x 7 days; B: 400 mg PO daily x 7 days; C: 600 mg PO daily x 7 days; D: 800 mg PO on day 1,400 mg PO daily on days 2-5. The solid grey region is the 90% prediction interval, the solid black line is the geometric mean, and the colored dots are observations stratified by individual. The average fold error (AFE) was calculated as $10^{\left(\frac{1}{n}\right)*\sum \log\left(\frac{\text{predicted}}{\text{observed}}\right)}$, where the predicted values were the simulated geometric mean values and n was the sample size. The AFE was 1.7, 1.1, 2.0 and 0.8 for the 200 mg, 400 mg, 600 mg PO daily and 800 mg followed by 400 mg PO plots, respectively.

Supplemental Figure 8. Population simulations for 100 mg, 200 mg, 400 mg, 800 mg oral single dose ketoconazole in adults.

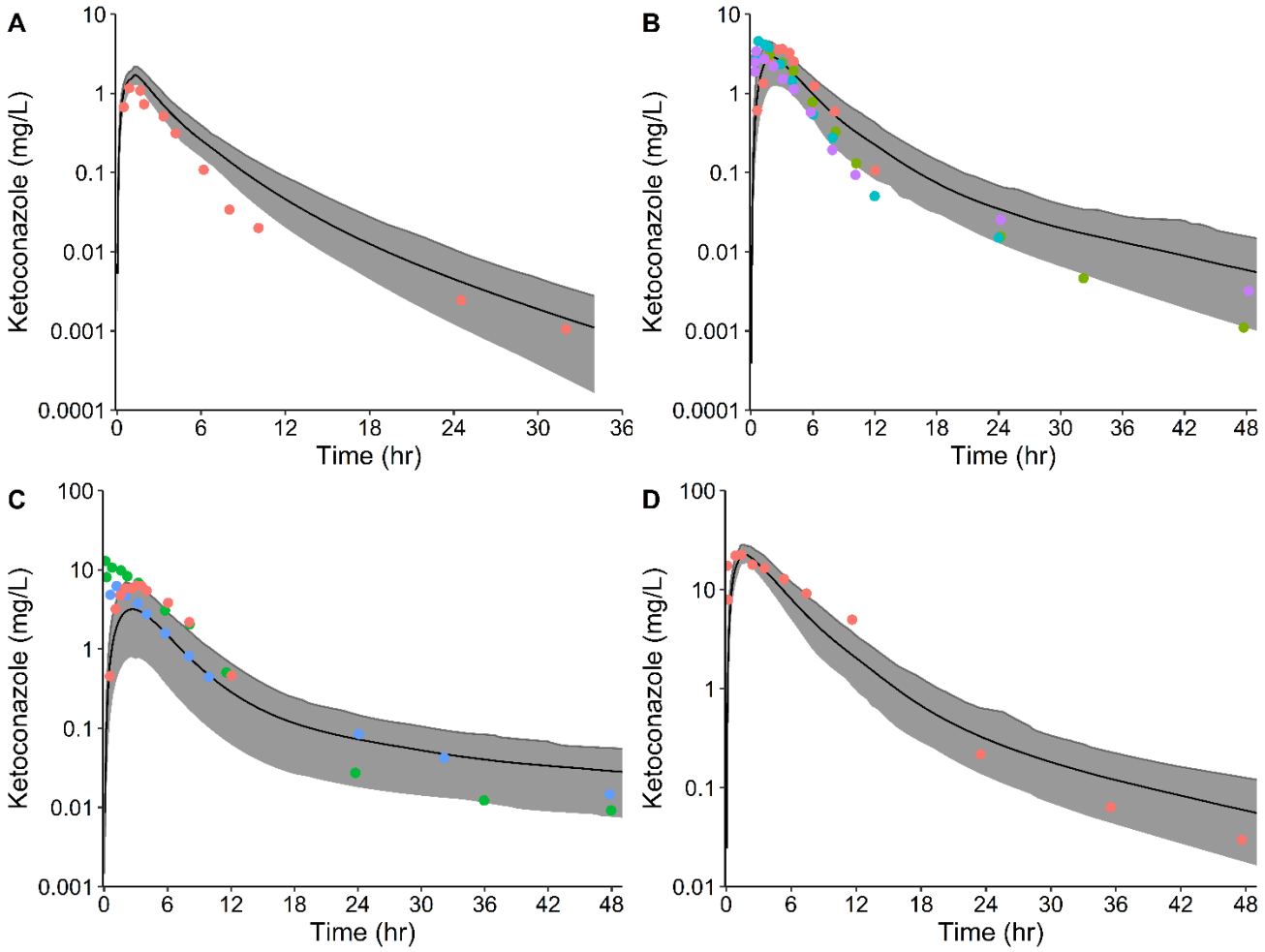

Population simulations based on 100 virtual subjects (white American population from 18 to 46 years of age) receiving 100, 200, 400, and 800 mg PO ketoconazole were performed. Single dose (A=100 mg PO, B=200 mg PO, C=400 mg PO, D=800 mg PO)

administration. The solid grey region is the 90% prediction interval, the solid black line is the mean, and the colored dots are the mean observations stratified by study. Observed data in orange is from healthy adults receiving a single dose of the oral solution of ketoconazole (Van Tyle, 1984). For the 200 mg PO simulation, the observed data in blue is from adults receiving the suspension, purple is from adults receiving the tablet, and green is adults receiving the solution formulation of ketoconazole (Huang *et al.*, 1986). For the 400 mg PO simulation, the observed data in green is from adults receiving the solution (Huang *et al.*, 1986) and the observed data in blue is from adults receiving the tablet formulation of ketoconazole (Daneshmend *et al.*, 1981).

Supplemental Figure 9. Population simulations for 200 mg and 400 mg oral multiple dose ketoconazole in adults.

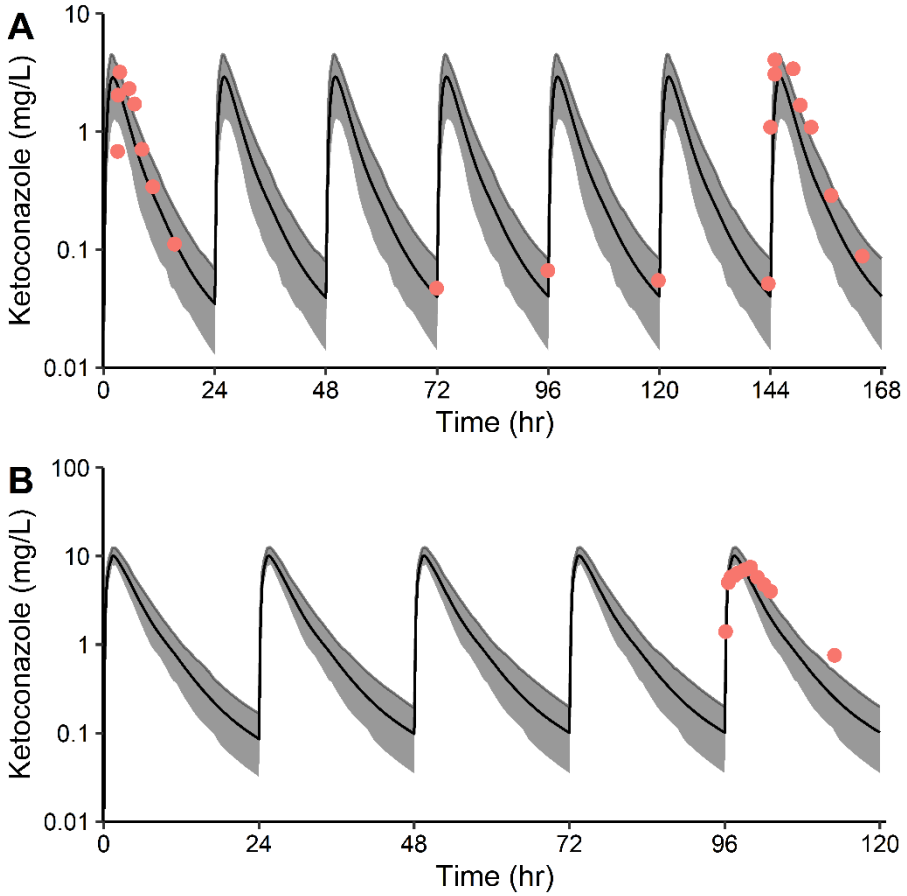

Population simulations based on 100 virtual subjects (white American population from 18 to 46 years of age) receiving 100, 200, 400, and 800 mg PO ketoconazole were performed. Multiple dose (A=200 mg daily x 7 days=A; B=400 mg daily x 5 days) administration. The solid grey region is the 90% prediction interval, the solid black line is the mean, and the colored dots are the mean observations

from clinical studies: 200 mg tablets once daily fasted for 7 days (Tiseo *et al.*, 1998) and 400 mg once daily for 5 days (Olkkola *et al.*, 1994).

Supplemental Figure 10. Population simulations for midazolam in adults.

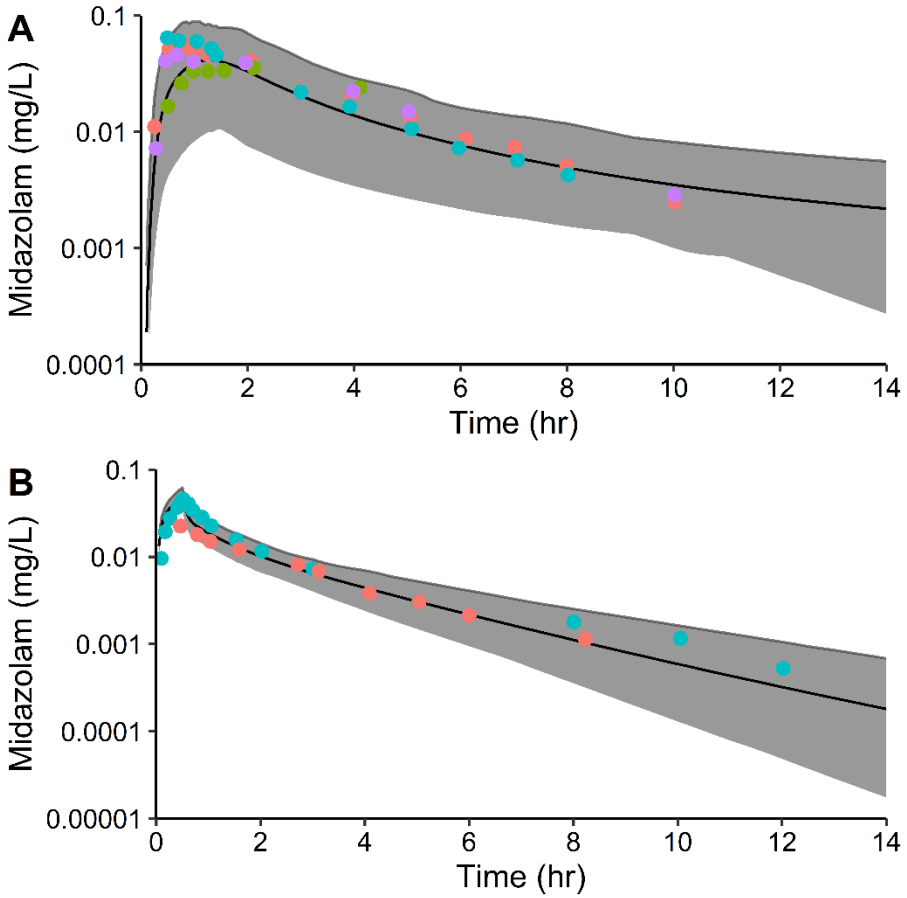

Population simulations based on 100 virtual subjects (white American population from 18 to 46 years of age) were performed. A: 15 mg oral (PO) midazolam single dose; B: 2 mg intravenous (IV) intravenous single dose. The solid grey region is the 90% prediction interval, the solid black line is the mean, and the colored dots are the mean observations from clinical studies. A: observed data in

healthy adults following a 15 mg oral tablet dose under fasting conditions (orange), one hour before a meal (blue), with a meal (purple), and one-hour after a meal (green) (Bornemann *et al.*, 1986). B: observed data from healthy adults receiving 2 mg IV midazolam over a 30 minute infusion, blue (Pentikis *et al.*, 2007) and orange (Tsunoda *et al.*, 1999).